Article (refereed) - postprint

Burman, Pramit Kumar Deb; Sarma, Dipankar; Morrison, Ross; Karipot, Anandakumar; Chakraborty, Supriyo. 2019. **Seasonal variation of evapotranspiration and its effect on the surface energy budget closure at a tropical forest over north-east India**.

Title: Seasonal variation of evapotranspiration and its effect on surface energy budget closure at a tropical forest over north-east India

Abbreviated running title: energy budget of a tropical forest over India

List of authors:-

Pramit Kumar Deb Burman[1, 4,*], Dipankar Sarma[2], Ross Morrison[3], Anandakumar Karipot[4], Supriyo Chakraborty[1]

Affiliations:-

[1]*Centre for Climate Change Research, Indian Institute of Tropical Meteorology, Pune - 411008, India*

[2]*Department of Environmental Sciences, Tezpur University, Tezpur - 784028, India*

[3]*Land Surface Science, Hydro-Climate Risks, NERC Centre for Ecology and Hydrology, Wallingford, Oxfordshire, OX10 8BB, United Kingdom*

[4]*Department of Atmospheric and Space Sciences, Savitribai Phule Pune University, Pune - 411007, India*

*Corresponding author. e-mail: pramit.cat@tropmet.res.in

Abstract

This study uses one year of eddy covariance flux observations to investigate seasonal variations in evapotranspiration and surface energy budget closure at a tropical semi-deciduous forest located in north east India. The annual cycle is divided into four seasons, namely: pre-monsoon, monsoon, post-monsoon, and winter. The highest energy balance closure (76%) is observed during pre-monsoon, whereas the lowest level of closure (62%) is observed during winter. Intermediate closure of 68% and 72% is observed during monsoon and post-monsoon seasons, respectively. Maximum latent heat flux during winter (150 W m^{-2}) is half of the maximum latent heat (300 W m^{-2}) flux during monsoon. Evapotranspiration is a controlling factor of surface energy budget closure, with highest rates of closure corresponding to the periods of highest evapotranspiration. The Bowen ratio ranges from 0.93 in winter to 0.27 during monsoon. This is the first time the role of evapotranspiration in the seasonal variation of surface energy budget closure has been reported for any ecosystem in north-east India using eddy covariance measurements.

Keywords: Eddy covariance; Indian summer monsoon; MetFlux India; Surface energy budget; Tropical forest; India

1 Introduction

India is one of the most populous countries of the world and is registering a fast and steady economic growth. As a predominantly agrarian economy, food production and economic activity depend strongly on the Indian summer monsoon (Gadgil and Gadgil, 2006). Apart from, ecosystem productivity, which is measured as the amount of carbon sequestered by ecosystems (Randerson et al., 2002), the dynamics of the monsoon also affects the hydrological cycle of the country. The Indian summer monsoon remains one of the most intriguing but least understood planetary-scale events, despite being subjected to active research over several decades (Goswami and Ajayamohan, 2001; Wang, 2006).

Evapotranspiration (ET; mm time period^{-1}) is a combined measure of evaporation and transpiration (Wang and Dickinson, 2012) which is the latent heat flux (LE; W m^{-2}) when expressed in energy units. Generally, ET is considered to have three components namely, water transpired by plants, and evaporation from soil and canopy-intercepted rainfall (Dirmeyer et al., 2006). Transpiration is a plant physiological process controlled by multiple physical and meteorological parameters such as precipitation (Giambelluca et al., 2009), soil water availability (Fisher et al., 2008), and radiation (Si et al., 2007). Forests in tropical regions are typically not water stressed due to a high annual rainfall (Pejam et al., 2006). Moreover, unlike arid and semi-arid regions, plant species have root systems that allow access to water in deeper soil layers (Scott et al., 2004; Yaseef et al., 2010). Hence, precipitation and/or soil moisture represent less important controls than available energy on ET in such regions.

Many studies have partitioned ET into transpiration and evaporative components using different methods, such as: stable isotope analysis (Rothfuss et al., 2010), sap flow techniques (Shuttleworth, 2007), as well as empirical and process models (Kool et al., 2014).

Several researchers have also studied relationships between the transpiration component and incoming photosynthetic photon flux density (PPFD; μmol photons m^{-2} s^{-1}) (Wilson and Baldocchi, 2000; Bovard et al., 2005).

ET represents one of the most important components of the hydrological cycle. Several recent studies have reported that ET from the Indian landmass is experiencing a decreasing trend in response to anthropogenic climate change (Jhajharia et al., 2009; Mukhopadhyay et al., (2017). At the smaller scale, ET has a strong dependence on land cover. Croplands and forest ecosystems, for example, have different ET dynamics due to contrasting biological responses to environmental conditions and management, such as soil water availability and irrigation scheduling, respectively (Wang and Dickinson, 2012). Modelling and observational studies show that ecosystems in the humid tropics have larger ET compared to ecosystems in other climatic regions (Fisher et al., 2009; Jung et al., 2011). Global ET studies (e.g. Jung et al., 2011) have also highlighted the strong ET flux from Indian ecosystems to the atmosphere, with dense areas of pristine forests in north east India showing particularly high rates. To date, such analyses in India have been based on coarse meteorological data and/or satellite derived products as higher temporal frequency, surface-based observations have not been available.

ET is an integral part of the surface energy budget. In India, there have been multiple field campaigns to study boundary layer evolution, surface fluxes, and their interactions with the Indian summer monsoon (Bhat and Narasimha, 2007). These experiments were primarily aimed at improving numerical weather forecasting models by providing improved momentum and sensible heat flux parameterisations. However, these campaigns were conducted over short time scales (MONTBLEX) (Sikka and Narasimha, 1995) and/or did not consider all components of the surface energy budget (LASPEX) (Vernekar et al., 2003). Based on a five month long tower-based observation around the monsoon period in Bangalore Bhat and

Arunchandra, (2009) reports that the longwave radiation and LE are largest sources of uncertainty in the surface energy budget closure. From a study conducted at Bangalore during the monsoons of 2009 and 2010, as part of the PROWNAM campaign Reddy and Rao, (2018) show the shortwave radiation and H to vary by 407 W m^{-2} and 126 W m^{-2} between the convective and non-convective conditions. The LE is found to be higher than H throughout a one year long measurement period during 1996-97 at Lucknow by Ramana et al., (2004).

More recently, the surface energy budget has been explored at a range of Indian ecosystems using different methodologies, such as, flux-gradient relationships, similarity theory or eddy covariance (EC) measurements. It is generally accepted the EC is currently the most defensible approach to quantify surface-atmosphere energy fluxes (Baldocchi, 2014); however, a key issue is a near-ubiquitous imbalance between EC-based observations of turbulent energy fluxes when compared against independent observations of the available energy (Leuning et al., 2012).

Several EC flux towers have now been established over different ecosystems across India (Jha et al., 2013; Rodda et al., 2016). Whereas diurnal, seasonal and inter-seasonal variations of water and carbon dioxide fluxes have been reported for several ecosystems, the dynamics of the surface energy balance have not been studied in detail. In other regions, EC analyses often divide the annual cycle into two contrasting periods, such as wet and dry (Eamus et al., 2001) or growing and post-harvest (Scott et al., 2004). For India, four distinct seasons have been classified, which are closely associated with the Indian summer monsoon (Wang, 2006). To the best of knowledge, no study has yet quantified the variation of surface energy budget closure according to these four seasons. Moreover, the influence of evapotranspiration measured from high-frequency, *in situ*, EC measurements on surface energy budget remains largely unexplored. Although the surface energy imbalance is nearly always observed in the EC-based studies none of the studies has explored this in detail.

MetFlux India is a project initiated by the Indian Institute of Tropical Meteorology (IITM) in Pune and funded by the Ministry of Earth Sciences (MoES), Government of India. It is inspired by Fluxnet the global network of EC flux towers (Baldocchi et al., 2001). Under MetFlux India, three new micrometeorological flux towers have been set up to monitor fluxes at forested ecosystems, including semi-deciduous forest in north east India, evergreen coniferous forest in the eastern Himalaya (Chatterjee et al., 2018), mangrove forest in the Bay of Bengal. Multi-year observations from MetFlux India stations will deliver long-term and continuous records of biosphere-atmosphere carbon, water, and energy fluxes.

The objectives of this study were: (1) to quantify seasonal variations of surface energy budget at a tropical semi-deciduous forest using the EC technique; (2) to enhance the surface energy imbalance by parameterising the soil heat flux and (3) to analyse the role of evapotranspiration as a control on seasonal variations in the level of surface energy budget closure.

2 Material and methods

2.1 Site

A 50 m tall micrometeorological tower (26°, 37' N and 93°, 21' E; Fig. 1) was established in Kaziranga National Park (KNP) in 2014 as part of a collaboration between IITM and Tezpur University. The flux observation site is a moist semi-deciduous forest with an average canopy height of 20 m. The climate is humid sub-tropical (CWa type) according to the Köppen classification scheme (Kottek et al., 2006). In this study, a one year record of fluxes and supporting micrometeorological observations from 2016 is analysed and reported. Full details of the site can be found in Deb Burman et al., (2017).

2.2 Instrumentation

The EC system was installed at measurement height of 37 m above the soil surface. The EC instrumentation consists of a WindMaster Pro 3-D sonic anemometer-thermometer (Gill Instruments, Lymington, UK), measuring zonal (u in m s^{-1}), meridional (v in m s^{-1}) and vertical (w in m s^{-1}) wind components at a temporal resolution of 10 Hz, combined with an LI-7200 enclosed path CO_2/H_2O Infrared Gas Analyzer (IRGA, Li-COR Biosciences, Lincoln, USA). Four WXT520 multi-component weather sensors (Vaisala Oyj., Vantaa, Finland) were installed at heights of 4 m, 7 m, 20 m and 37 m, each providing measurements of ambient air temperature (T_a in K), air pressure (P in hPa), rainfall (precip in mm) and relative humidity (RH in %) at 1 minute intervals. Soil temperature (T_s in K) and moisture content (SWC in m^3 m^{-3}) were recorded every 1 min by 5TE water content, electrical conductivity and temperature sensors installed at five different depths (surface, 0.05 m, 0.15 m, 0.25 m and 0.40 m). Two HPF01SC-20 soil heat flux plates (HukseFlux, Manorville, USA) were installed at the depth of 0.05 m for measuring the ground heat flux (G in W m^{-2}) every minute. Net radiation (R_n in W m^{-2}) and its four components, namely incoming shortwave radiation (R_{SW}(in) in W m^{-2}), incoming longwave radiation (R_{LW}(in) in W m^{-2}), outgoing shortwave radiation (R_{SW}(out) in W m^{-2}) and outgoing longwave radiation (R_{SW}(out) in W m^{-2}) were measured every 1 min by a NR01 4-component net radiometer (HukseFlux, Manorville, USA). PPFD in µmol m^{-2} s^{-1} was measured every 1 min by a SQ-110 Sun calibrated quantum sensor (Apogee Instruments Inc., Logan, Utah, USA). These two instruments were installed at a height of 19 m on the tower. Additionally, half-hourly averaged records of all variables were also created and logged using two CR3000 data loggers (Campbell Scientific, Logan, Utah, USA). Details of the above-mentioned instrumentation and variables are summarised in Table 1.

2.3 Data handling

2.3.1 Flux calculation from EC data

Sensible (H in W m^{-2}) and latent (LE in W m^{-2}) heat fluxes are computed from the raw EC data following Reynolds averaging (Aubinet et al., 2012) using EddyPro version 6.2.0 (https://www.licor.com). High frequency measurements by the EC system are often contaminated by various types of error that require corrections (Burba, 2013) such as, obtrusive angle of flow, random spikes, instrumental offset, non-ideal geometry etc. These errors originate from multiple different reasons ranging from instrumental limitations to faulty experimental set up. Hence, before computing fluxes, raw EC data are subjected to rigorous quality control measures, including angle of attack correction (Nakai et al., 2006), despiking (Mauder et al., 2013), block averaged detrending (Kaimal and Finnigan, 1994) and dual-axis coordinate rotation (Kaimal and Finnigan, 1994). Due to the physical separation between the sonic anemometer and IRGA a time lag is introduced between the measured wind components and gaseous mixing ratios (c and q) which is compensated by applying a time lag correction (Burba, 2013). High (Moncrieff et al., 2005) and low-pass corrections (Moncrieff et al., 1997) are applied to compensate for the loss of flux towards the low and high frequency ranges of the cross-spectrum, respectively. Such losses can arise out of the inefficient filtering and/or time averaging (Burba, 2013).The WPL correction (Webb et al., 1980) was applied while calculating fluxes from the gaseous mixing ratios to remove the effect of humidity and temperature.

2.3.2 Post-processing and quality control of flux data

Half-hourly averaged values of T_a, Ts, RH, SWC, R_{SW}(in), R_{LW}(in), R_{SW}(out), R_{LW}(out), R_n, PPFD and G are aggregated into biometeorological file to be used as additional input to EddyPro. These variables are measured with lower time resolution than EC. Full output of EddyPro contains these biometeorological variables, averaged and time

synchronised with calculated fluxes. Random uncertainties arising out of the flux sampling error are computed following Finkelstein and Sims, (2001). A daily quality control file is also generated along with the fluxes., containing statistical parameters and flags for stationarity and well developed turbulence tests for the calculated fluxes (Foken et al., 2004). Outliers in H and LE data were detected and removed by the median absolute deviation (MAD) (Sachs, 1997) technique and removed following Papale et al., (2006).

2.3.3 Gap-filling of flux and meteorological data

Long term records of meteorological and flux variables inevitably experience data gaps related to sensor or system malfunctions, unfavourable measurement conditions or insufficient power, as well as data filtering during QC (Moffat et al., 2007). In this study, flux data gaps are filled using the REddyProc Package (Wutzler et al., 2018) for the R Language (R Core Team). It offers various mechanisms to be applied for filling the gaps. In the present work, the marginal distribution sampling (MDS) approach (Reichstein et al., 2005) is used to fill gaps in H, LE, R_n, R_{SW}(in), G and PPFD.

2.3.4 Parameterisation of soil heat flux

Soil heat flux (G) is an important component of the surface energy budget. It is directly measured by soil heat flux sensors installed within the top soil layer. The observation of G suffers from frequent data loss due to water logging, power failure, sensor damage and malfunctioning (Sauer et al., 2007) and the underestimations in G result in non-closure of the SEB (Heusinkveld et al., 2004). Attempts have been made by several researchers to address this potential problem by indirect estimates of G. Remote sensing based estimates of G were compared against a set of distributed soil heat flux plates by Daughtry et al., (1990), Kustas and Daughtry, (1990). It was seen to reduce the error in SEB significantly. Other such methods include calculating G from soil temperature and moisture (Yang and Wang, 2008),

from relationships with vegetation indices (Kustas et al., 1993), correcting G in conjunction with Bowen ratio method (de Silans et al., 1997) etc.

The forest floor at KNP remains waterlogged during most of the monsoon and post-monsoon seasons due to heavy and frequent rainfall. Due to the presence of dark cumulus clouds and dense vegetation canopy least amount of sunlight penetrates through the forest. Such conditions resulted in insufficient charging of the solar cells causing power shortage. As direct electricity connection could not be provided within the forest, all instruments and sensors are powered by the solar cells. Hence, during most of the times in monsoon and post-monsoon, sensors remain inactive and frequent long data gaps are observed in G. For filling up the longer gaps in G a simplistic parameterisation scheme is devised between R_n and G as Purdy et al., (2016) shows that such schemes are widely used in globally and better-suited to capture the high-frequency variations compared to the other schemes.

The boundary between day- and night-time conditions was defined using $R_{SW}(in) \geq 20$ W m^{-2} and $R_{SW}(in) < 20$ W m^{-2}, respectively. This is an objective criterion based on Reichstein et al., (2005). Following this, available half-hourly data are divided into daytime and nighttime. For both of these times, scatter plots are made between R_n and G. Assuming a linear relationship between R_n and G (Idso et al., 1975; Norman et al., 2000), two different straight lines are fit to these scatter plots. These straight line fits are further separately used for interpolating G using R_n during daytime and nighttime. Finally, daytime and nighttime values are merged together to create a continuous half-hourly record of G.

2.3.5 Calculation of vapour pressure deficit (VPD)

Vapour pressure deficit (VPD) is defined as the difference between saturation water vapour pressure and measured water vapour pressure at a given air temperature (Monteith, 1965). It is a measure of the moisture holding capacity of the atmosphere at that particular

temperature (Wang and Dickinson, 2012). We have calculated VPD from T_a and RH using REddyProc. Existing gaps in T_a and RH propagate in VPD which are filled by the MDS algorithm using REddyProc.

2.3.6 Seasonal variation

To analyse seasonal patterns, observations obtained during 2016 were divided into four seasons; namely, monsoon, post-monsoon, winter and pre-monsoon. The Indian landmass gets immensely heated up during summer due to the enhanced amount of incoming solar radiation. This results in a distinct land ocean temperature gradient (Xavier et al., 2007). As a result, moisture-laden south-westerly wind flows into the peninsular India from the Arabian Sea bringing in an enhanced amount of rainfall. According to Wang and Ho, (2002) the total annual rainfall is concentrated in the months of summer (June, July, August and September, abbreviated as JJAS), often identified as the monsoon. Monsoon withdrawal takes place in the month of October (Wang, 2006).

The months after withdrawal of Indian summer monsoon are characterized by receding amount of rainfall and decreasing temperatures (Jain and Kumar, 2012). Hence the months of October and November, abbreviated as ON are defined as post-monsoon (Hingane et al., 1985; Singh et al., 2000). Winter is defined as the months of December, January and February, abbreviated as DJF (Hingane et al., 1985). During this period, the land-ocean temperature gradient is reversed due to the cooling of the land caused by a decreased amount of incoming solar radiation. This results in reversal of the near-surface wind over the Indian landmass (Wang, 2006). Annual minimum air temperature is observed during these months (Jain and Kumar, 2012). This is also the driest period of the year recording the minimum amount of rainfall (Parthasarathy et al., 1994). Air temperature starts rising in the month of March and continues the increasing trend till the end of May causing an intense heating of the

Indian landmass in the process. Pre-monsoon heating plays a crucial role in reversing the land ocean temperature gradient and total amount of rainfall over all India during monsoon (Parthasarathy et al., 1990). Monsoon onset takes place in the first week of June. Hence, the months of March, April and May, abbreviated as MAM is defined as pre-monsoon (Hingane et al., 1985; Jain and Kumar, 2012).

2.3.7 Surface energy budget and Bowen ratio

The surface Energy Budget (SEB) is the manifestation of the conservation of energy at the Earth's surface. Net radiation (R_n) reaching Earth surface is calculated from the incoming and outgoing radiation components, using:

$$R_n = R_{SW}(in) + R_{LW}(in) - R_{SW}(out) - R_{LW}(out), \quad (1)$$

where all variables were defined above. R_n is further partitioned into sensible (H), latent (LE) and soil (G) heat fluxes, as:

$$R_n = H + LE + G, \quad (2)$$

Complete energy balance closure (e.g. energy conservation) should result in a linear relationship with a slope of unity for (R_n - G) versus (H + LE) (Stull, 2012). However, full closure is rarely met using EC measurements due to unaccounted energy fluxes from advection, heat storage in air, soils and biomass. (Leuning et al., 2012; Burba, 2013), as well as larger scale atmospheric motions (Fisher et al., 2008). This energy imbalance can translate either to an overestimation of H and LE or an underestimation of R_n (Aubinet et al., 2012), and either of these erroneous estimates is reflected by the y-intercept of the SEB scatter plot. In this study, energy balance closure is reconstructed and analysed for each of the four seasons and the y-intercept of the SEB scatter plot is referred to as the residual energy in rest of this manuscript.

The Bowen ratio (β) is defined as the ratio of sensible to latent heat fluxes (Tanner, 1960), as:

$$\beta = H/LE, \quad (3)$$

The Bowen ratio has been widely used for estimating LE from observations of H (Dugas et al., 1991; Shi et al., 2008) following the assumption of full SEB closure (Malek and Bingham, 1993; Twine et al., 2000; Gu et al., 2005; Tsai et al., 2010; Cho et al., 2012). Generally, midday value of β is preferred for the analyses (Jarvis et al., 1997) as maximum values of H and LE are observed around midday. For the present work, Table 3 lists the seasonal values of SEB closure, residual energy and β.

3 Results

Annual meteorology at KNP for 2016 is shown in Fig. 2. Half hourly records of T_a, P and precip are available at four different heights (Table 3). For each of these variables, the mean of the four records is calculated. Further, daily averaged values of T_a and P have been calculated from their average half-hourly records. Daily total values of precip are calculated by summing up its average half-hourly record over the duration of each day. Figs. 2 (a), (b) and (c) show daily values of T_a, P and precip respectively, calculated this way.

Prominent seasonal variations are seen in each of the three variables mentioned above. Annual minimum and maximum T_a are 285 K and 305 K which are recorded in winter and monsoon, respectively. T_a starts increasing towards the end of winter and continues rising during pre-monsoon. Ta attains a peak values during monsoon and starts decreasing by the end of monsoon. A sharp decline is observed in T_a during post-monsoon. Unlike pre-monsoon and post-monsoon, T_a remains stable in monsoon and does not change rapidly with time. Finally, T_a drops down to its minimum value in winter.

P showed a rapid declines and growth during pre-monsoon and post-monsoon, respectively. Maximum P (Fig. 2) was observed during winter (1010 hPa). P decreased continuously in pre-monsoon and attained a minimum value of 990 hPa during monsoon. P increased during post-monsoon. Annual pattern of P shows opposite trends to T_a. Similar to T_a, P remained stable with low variability during monsoon.

Winter is the driest season at KNP with negligible amount of rainfall observed during this season. KNP started receiving rainfall in April, with daily values of around 75 mm recorded during April and May. The monsoon season experiences the highest amounts of rainfall, with values of 100 mm day^{-1} observed during this period. Daily rainfall totals start decreasing towards the end of monsoon, with fewer more isolated rainfall events observed during the post-monsoon season.

The scatter plot of half-hourly records of R_n and LE for the entire measurement period is presented in Fig. 3. As expected, LE increases with increasing R_n. As a first approach towards evaluating the SEB, the long data gaps in G are ignored. This way the linear fit between the available energy (R_n - G) and the sum of the turbulent energy fluxes (LE+H) (Fig. 4) is statistically significant, and shows that SEB closure is 69% ($y = 0.69x + 9.89$, Adjusted $R^2 = 0.84$, $p < 0.05$), with an energy imbalance of 31%.

In order to improve the SEB closure, G is parameterised using the method described in 2.2. A linear relationship is assumed between G and R_n throughout the day, with different slope and intercepts for day and night-time. Differences between day and night reflect lower turbulent energy exchanges relative to daytime conditions. For daytime conditions, a linear fit indicated that G increases by 2.5% of R_n ($y = 0.025x + 0.22$, $p < 0.05$). For nocturnal conditions, G decreases by 3.2% of Rn ($y = -0.032x - 5.24$, $p < 0.05$).

Remaining day- and night-time gaps in G are filled using the relationships described above. This gap-filled record of G is referred to as parameterised G, and is used to represent soil heat fluxes for the remainder of the manuscript unless indicated otherwise. The linear fit between the available energy (calculated using parameterised G) and the turbulent energy fluxes ($y = 0.70x + 10.36$, Adjusted $R^2 = 0.87$, $p < 0.05$) shows closure increases by 1% compared to the previous fit. Daily averaged values of R_n, G, H and LE are calculated from their half-hourly records. The linear fit to the daily values indicated SEB closure of 80% ($y = 0.8x + 0.04$, Adjusted $R^2 = 0.87$, $p < 0.05$), improving SEB closure by 10% compared to linear fits based on 30 minute observations.

Mean diurnal variations of R_n, R_{SW}(in), H and LE during pre-monsoon (MAM), monsoon (JJAS), post-monsoon (ON) and winter (DJF) are presented in Fig. 8. Prominent seasonal variation is observed in R_n. Maximum values of R_n during pre-monsoon, monsoon, post-monsoon and winter are approximately 500, 550, 525 and 400 W m^{-2}, respectively. Negative values of R_n are observed during nighttime. The most negative R_n is observed during winter and the least negative values are observed in monsoon. Closer inspection of the diurnal variations reveala that during winter R_n starts increasing around 6.5 h, becomes positive around 7.5 h, reaches maximum around 11.0 h and starts decreasing thereafter. Whilst decreasing it becomes zero around 16.0 h. It reaches a minimum value of -50 W m^{-2} at 17.5 h. On the other hand, during monsoon R_n starts increasing around 5.0 h, became positive at 6.0 h, reaches maximum at 12.5 h and onwards starts decreasing. It becomes zero at 18.0 h while decreasing and reaches a minimum value of -25 W m^{-2} at 19.0 h. During pre-monsoon R_n starts increasing around 5.5 h, becomes positive around 6.5 h, reaches maximum around 12.0 h and starts decreasing onwards. It becomes negative at 17.5 h and reaches a minimum value of -30 W m^{-2} around 18.5 h. Finally, during post-monsoon R_n registers an increasing trend around 5.5 h, becomes positive around 6.0 h, reaches maximum around 12.0 h and

onwards starts decreasing. While decreasing, it become negative at 16.0 h and records minimum value around 17.5 h.

The maximum values of R_{SW}(in) during pre-monsoon, monsoon, post-monsoon and winter are 625, 650, 650 and 550 W m^{-2}, respectively (Fig. 8). R_{SW}(in) remains zero during nighttime throughout the seasons. During winter it starts increasing around 6.0 h, reaches maximum around 12.5 h and decreases to zero around 18.0 h. On the other hand, during monsoon, R_{SW}(in) starts increasing around 5.5 h, reaches maximum around 13.0 h and decreases to zero around 19.0 h. During pre-monsoon R_{SW}(in) starts increasing around 5.5 h, reaches maximum around 12.0 h and decreases to zero around 19.0 h. Finally, during post-monsoon R_{SW}(in) starts increasing at 6.0 h, reaches maximum around 11.0 h and decreases to zero around 17.5 h.

The maximum values of H that are observed during different seasons are, 100 W m^{-2} during pre-monsoon, 85 W m^{-2} during monsoon, 110 W m^{-2} during post-monsoon and 140 W m^{-2} during winter (Fig. 8). Throughout the seasons, H is positive during daytime and negative during nighttime. During pre-monsoon, minimum value of H is -20 W m^{-2} which is recorded at night. It increases and becomes positive at 7.5 h. It reaches the maximum value at 12.0 h and starts decreasing onwards. While decreasing it becomes negative at 16.0 h. During monsoon H records a minimum value of -10 W m^{-2} at night. It becomes positive around 6.0 h. It remains maximum till 13.0 h from 11.0 h. Further, it starts decreasing and becomes negative around 17.0 h. During post-monsoon H remains negative but close to zero during nighttime. It increases and becomes positive around 6.0 h. It further increases and becomes maximum around 11.0 h. It decreases onwards and becomes negative around 16.0 h. In winter, during nighttime H remains more negative than monsoon but less negative than post-monsoon. It increases and becomes positive around 9.0 h. Maximum value of H is reached at 13.0 h. After that H starts decreasing and becomes negative at 16.0 h.

A maximum value of 300 W m^{-2} is observed for LE during pre-monsoon, monsoon and post-monsoon (Fig. 8). During winter, maximum LE is reduced to 150 W m^{-2}. LE is close to zero during nocturnal periods for post-monsoon and winter seasons. LE remains non-zero and positive during night-time during the monsoon and post-monsoon period. During pre-monsoon, LE starts rising at 6.0 h, reached a maximum at 12.0 h and starts decreasing thereafter. It reaches a minimum value of 25 W m^{-2} at 19.0 h which is maintained for the rest of the night. In quite a similar fashion, LE starts increasing around 6.0 h during monsoon. However, it reaches maximum value around 12.5 h. Further, it records a decreasing pattern and obtains a minimum value of 25 W m^{-2} around 19.0 h. This minimum value is maintained throughout the night. For a long-time it was thought that transpiration stops at night due to the stomatal closure in the absence of solar radiation (Dawson et al., 2007; Wang and Dickinson, 2012). However, several studies confirmed that nighttime respiration form a significant component of the total transpiration. Nighttime transpiration is stronger in plants and crops that are grown in water unstressed environment (Caird et al., 2007; Novick et al., 2009). During post-monsoon LE starts increasing around 9.0 h, reaches maximum around 12.0 h and decreases onwards. It drops to the minimum value of 15 W m^{-2} at 18.0 h which is maintained throughout the rest of the night. During winter LE starts increasing at 7.5 h and reaches maximum at 13.0 h before dropping to a minimum of zero at 18.0 h.

Half-hourly components of SEB are estimated separately for different seasons. SEB is computed for each of the seasons using Eq. 2. Scatter plots between (R_n - G) and (H + LE) for pre-monsoon, monsoon, post-monsoon and winter have been shown in Fig. 9. Panels (a), (b), (c) and (d) of Fig. 9 correspond to pre-monsoon, monsoon, post-monsoon and winter, respectively. For each of the seasons, linear relationships are fit by least-square method in R to the scatter plots which are also shown in these figures. Equations governing these fits and the corresponding adjusted R-square values are provided on Fig 9.

High R-square values (Fig. 9) show that all the fits are representative of the interrelations among SEB components. Highest (76%) and lowest (62%) SEB closures are obtained during pre-monsoon and winter (Fig. 9), respectively. Intermediate SEB closure is observed during monsoon (68%) and post-monsoon (72%). Residual energy that is partitioned into (H + LE) but unaccounted in (R_n - G) is maximum during winter which is 15.55 W m^{-2}. It is comparable to post-monsoon when residual energy remains at 15.36 W m^{-2}. However, this residual energy is minimum at 5.11 W m^{-2} during monsoon. During pre-monsoon residual energy stands at 8.53 W m^{-2}. Seasonally mean midday β is maximum at 0.93 during winter and minimum at 0.27 during monsoon, respectively. β has intermediate values of 0.33 and 0.37 during pre-monsoon and post-monsoon, respectively.

The PPFD is one of the major drivers of photosynthesis which is closely coupled with the transpiration by stomatal control mechanism in plants (Sellers, 1987). Increased availability of PPFD accelerates the photosynthesis and hence transpiration. In this paper the evapotranspiration is not partitioned into evaporation and transpiration. However the LE is analogous representation of the evapotranspiration. In order to get an overall estimate of the seasonal dependence of evapotranspiration on PPFD, scatter plots between the half-hourly values of PPFD and LE are plotted in Fig. 10. Straight lines are fit to these plots and the corresponding fit parameters are given in the figures.

Atmospheric VPD is another major driver of evapotranspiration. In order to compare the control of VPD on evapotranspiration among different seasons, the scatter plots between half-hourly values of LE and VPD are plotted by season in Fig. 11. All the plots show clear clockwise temporal trends. To explain the role of VPD in the growth of LE, fits are made to the increasing part of these relationships. These fits are also shown in the same figure.

During pre-monsoon, minimum and maximum recorded values of VPD are 2.5 hPa and 16 hPa, respectively. Minimum value of LE during pre-monsoon is negligible but non-zero. LE increases to its maximum value of 300 W m^{-2} in a non-linear fashion till VPD grows up to 13 hPa. VPD increases further to 16 hPa with a continuous non-linear decrease in LE till 200 W m^{-2}. Further, VPD decreases continually to 3 hPa with an associated non-linear decrease in LE.

During monsoon, minimum and maximum values of VPD are 3 hPa and 15 hPa, respectively. Minimum value of LE is small but positive during this season. This minimum value of LE is observed when VPD is at its minimum. Initially, LE increases linearly to its maximum value with VPD till 13 hPa. VPD records a further growth till 15 hPa beyond this point. During this phase, LE drops to 200 W m^{-2} in a non-linear fashion. Finally, LE decreases non-linearly with VPD to their minimum values.

In post-monsoon, minimum and maximum values of VPD are 1.5 hPa and 16 hPa, respectively. Minimum value of LE during this season is zero. Initially, LE increases non-linearly with VPD. LE gets saturated at 275 W m^{-2} when VPD reaches 10 hPa. LE maintains this saturation value with further increase in VPD, till 14 hPa. LE starts decreasing with VPD beyond this value. VPD grows till 16 hPa with an associated continuous decrease in LE till 200 W m^{-2}. LE further decreases non-linearly with VPD to their minimum values.

In the season of winter, minimum and maximum values of VPD are 1 hPa and 15 hPa, respectively. Initially, LE records a non-linear growth with VPD. LE gets saturated to 150 W m^{-2} when VPD becomes 10 hPa. This saturation value of LE is maintained till VPD reaches 13 hPa. VPD further grows to 15 hPa during which a continuous non-linear decrease is observed in LE. Finally, LE decreases with VPD in a non-linear fashion to their minimum values.

Initially in all the seasons, LE is seen to increase with VPD. Gradually, LE reaches a maximum value beyond which it starts decreasing. LE always decreases with decreasing VPD. It has a very non-linear effect on LE due to two related but opposite mechanisms. VPD is the pressure difference felt by the water vapour within the plant body with respect to the outside atmosphere. This pressure difference drives the transport of the water vapour through the plant body and eventually its release into the atmosphere through the stomata in the form of transpiration. Hence, more the VPD more is the LE. On the other hand, higher VPD inhibits stomatal conductance. This is a negative effect resulting in the stomatal closure and lower LE. At lower values of VPD, positive effect remains stronger (Bréda, 2003). Hence LE increases with VPD. Eventually, LE reaches a maximum value after which it starts decreasing. This decreasing effect is due to the strong control of VPD on stomatal conductance at higher values (Gu et al., 2005). However, the critical value of VPD at which this transition happens is not fixed and depends on multiple meteorological variables.

4 Discussion

In this work we aimed to study the seasonal variation of surface energy budget closure at a tropical forest over north-east India and to improve the imbalance using a simple parameterisation scheme of G. Additionally we also studied the role of ET on the surface energy balance in different seasons. We have parameterised G from R_n assuming a linear relationship. Averaged over a daily scale the net heat flux from ground is often close to zero. It translates to the fact that heat gain by the soil during daytime is near exactly balanced by the heat loss during night. Additionally, as soil has very poor heat capacity, net change in the heat stored in soil during a day is zero (Stull, 2012). G constitutes a larger portion of R_n during nighttime compared to daytime. This is the manifestation of the fact that H and LE are much smaller during nighttime compared to daytime. Hence, more energy is partitioned into

G during nighttime. With a reference to this, daytime and nighttime relations between G and R_n are treated separately. As shown earlier, 3.2% of R_n is partitioned into G as compared to 2.5% during daytime. During nighttime incoming shortwave and longwave radiations (R_{SW}(in) and R_{LW}(in), respectively) are absent. However, Earth loses heat by outgoing longwave radiation (R_{LW}(out)) which results in cooling of the ground. This is also evident from the negative values of R_n during nighttime. Due to poor heat retentivity, ground loses heat and gets cooler as night progresses. In other words, R_n is driven at the cost of G. Hence, a negative slope between G and R_n is seen during nighttime.

The half-hourly values of G, gap-filled by interpolating the linear dependence on R_n enhance the SEB closure by 1%. Till date, a complete closure of SEB using half-hourly values measured from EC and other supportive measurements could not be achieved by the scientific community (Aubinet et al., 2012). Typically, 70% - 90% closure is reported by various flux measurement groups over multiple different ecosystems and terrains across the globe (Anderson et al., 2000; Wilson et al., 2002; Leuning et al., 2012). Over a mixed deciduous forest plantation at Haldwani, Watham et al., (2014) reports the surface energy budget closure to vary approximately within 60% to 80% among different months without considering G during a 9 month long observation from January to September, 2013. Many corrections have been proposed for improving the estimates from high-frequency EC measurements resulting in very little or no improvement. It is assumed that this non-closure of SEB has little to do with the post-processing techniques associated with EC as rectifications proposed for EC flux measurement have reached the maximum level of accuracy (Mauder and Foken, 2006). SEB often results in a better closure, if calculated in a larger temporal scale (Jarvis et al., 1997; Sakai et al., 2001). In the present work, daily-averaged values of R_n, H, LE and G are seen to result in 80% closure of SEB. Thus, there is a 10% enhancement in SEB closure. Erroneous estimation of SEB components is also seen to

reduce to 0.04 W m^{-2} at daily scale, from 10.36 W m^{-2} at half-hourly scale. Clearly there is a 259 times improvement in the estimation of SEB components.

Distinct change in the vegetation cover is observed among the different seasons at the semi-deciduous forest at KNP. The Leaf Area Index (LAI) changes from a minimum value of 0.75 in winter to a maximum value of 3.25 in monsoon (Deb Burman et al., 2017). Gradually increasing and decreasing trends are observed in LAI during pre-monsoon and post-monsoon, respectively. Changes in LAI have deep impact on the transpiration by forest canopy (Bréda, 2003; Wang and Dickinson, 2012). Additionally annual maximum R_n is 550 W m^{-2} observed during this season (Fig. 8). It decreases in post-monsoon and reaches minimum at 400 W m^{-2} in winter to increase subsequently in pre-monsoon.

Combined together, these features result in enhanced LE during monsoon. More R_n is partitioned into LE as evident from Fig. 8. Winter is dry over KNP. Maximum LE during this season is 150 W m^{-2} which is half of the maximum LE during monsoon. Additionally, in winter LE drops to zero during nighttime which is not the case in monsoon. On the other hand, H is maximum at 140 W m^{-2} in winter and minimum at 80 W m^{-2} in monsoon. Hence, it can be seen that the share of LE in R_n is maximum in monsoon and minimum in winter. This is supported by a study by Brümmer et al., (2008) in which the differential responses of shrub savanna during dry and wet seasons were studied. Proportion of LE in R_n increases during pre-monsoon as moisture laden air starts entering the landmass. Contradictorily, it decreases during post-monsoon as this moist airmass gradually recedes from the landmass.

These observations suggest that SEB closure needs to be carefully examined for each season as relative strengths of different SEB components vary widely from one season to another. These changes are brought in by different physical, dynamical and physiological processes those may not be resolved in annual scale (Ramier et al., 2009). As seen in the

present work, best and worst closures of SEB are 76% and 62% which are observed during pre-monsoon and winter, respectively. Intermediate closures of 68% and 72% are seen in monsoon and post-monsoon, respectively. Residual energy is minimum in monsoon at 5.11 W m^{-2}, and maximum in winter and post-monsoon at 15.55 and 15.36 W m^{-2}, respectively. Residual energy during pre-monsoon remains at 8.53 W m^{-2}. These observations show that with least evapotranspiration happening, worst closure is achieved during winter which also increases the magnitude of residual energy. This is can be explained as follows. During winter a significant proportion of R_n gets channelised into other components which can not be directly measured and hence are not included in SEB. Such components may include canopy storage, absorbed radiation etc (Aubinet et al., 2012). These losses in R_n are reflected as the residual energy.

On the other hand, with more evapotranspiration happening during monsoon a major chunk of R_n is partitioned into LE which is measured with good confidence (Mauder and Foken, 2006; Foken et al., 2011). This brings down the residual energy that accounts for the various losses. As a result, better SEB closure is observed in monsoon. Pre-monsoon and post-monsoon both are the transitive phases between monsoon and winter with the difference being the gradual increase and decrease in the temperature of the atmospheric air column. This can be seen from the greater magnitude of H during pre-monsoon over post-monsoon. LE is similar to monsoon in both of these seasons. With more R_n being partitioned into LE, SEB closures better than winter are observed in these two seasons. Seasonal variation of residual energy has a same pattern as β as seen from Table 3. Maximum and minimum values of β result in largest and smallest values of the residual energy, respectively. It suggests that the closure of SEB is linked with the relative partitioning of energy between H and LE. More is the value of LE, less is β and hence better is the SEB closure. Hence, evapotranspiration is seen to have a decisive role in the variation of SEB closure among different seasons.

In order to further investigate the role of LE in SEB closure the relation between LE and PPFD in different seasons has been studied. However, LE has not been separated into evaporation and transpiration as our objective in this study remains not to study the interrelationship between these two which is a complex biogeochemical process (Lawrence et al., 2007) but to assess their combined impact on SEB among different seasons. LE increases with PPFD during all the seasons. Increased PPFD results in enhanced photosynthetic activity by plants (Frolking, 1998; Reverter et al., 2010). This in turn triggers transpiration as it is closely coupled with photosynthesis (Wang et al., 2006). Linear fits between LE and PPFD have adjusted R-square values of 0.87, 0.83, 0.85 and 0.81 in pre-monsoon, monsoon, post-monsoon and winter, respectively. Similar finding have been reported by Greco and Baldocchi, (1996); and Pieruschka et al., (2010) where transpiration changed proportionately with PPFD. The slope between LE and PPFD remains similar during pre-monsoon, monsoon and post-monsoon which are 0.26, 0.22 and 0.23, respectively. However, it is markedly different at 0.15 during winter. Being deciduous, the forest at KNP shed leaves during winter. This is evident from the LAI value of the canopy which drops down to a mere 0.75 in winter from 3.25 in monsoon (Deb Burman et al., 2017). Hence, during winter an increase in PPFD does not increase transpiration much. That is why the PPFD has overall less control on evapotranspiration.

Marked differences are found in the pattern of variation of LE with VPD among different seasons at KNP. In all the seasons, LE grows initially with VPD during day time. However, it starts decreasing after VPD reaches a critical value. On the other hand, LE decreases monotonically in a non-linear fashion with VPD during night time in all the seasons. Such type of behaviour exhibits a clear hysteresis pattern quite similar to the one reported by Hogg and Hurdle, (1997) and Gyenge et al., (2003). Growth of LE at lower values of VPD can be attributed to enhanced transpiration as explained by Gu et al., (2006).

However, after a critical value of VPD, stomatal closure takes place in the plants causing the cessation of sap flow (Anthoni et al., 2002; Fisher et al., 2007). As a result of this transpiration saturates and eventually starts decreasing. KNP being a densely vegetated tropical forest, transpiration dominates the evapotranspiration process (Jasechko et al., 2013). However, during monsoon atmosphere becomes significantly more humid than the other times of the year. As a result, evaporation is stronger in monsoon than three other seasons. This is seen from the minimum values of VPD observed in different seasons. In monsoon, VPD never falls below 3 hPa whereas in winter it reaches as low as 1 hPa. Annually, minimum and maximum VPD are observed in winter and post-monsoon, which are 1 hPa and 16 hPa, respectively. Due to increased availability of moisture in monsoon, LE records a linear growth with VPD as seen from Fig. 11(b). Similar behaviour have been found by Goldstein et al., (2000) and Admiral et al., (2006). Being a deciduous forest, KNP records lowest annual LAI in winter (Deb Burman et al., 2017). It is also the driest period of the year as the available moisture content in the atmosphere remains lowest in this season. As a result, both evaporation and transpiration are hindered. Hence, LE saturates to the lowest value in winter among all the four seasons. With the advent of monsoonal wind rich in water vapour, gradual increase in atmospheric moisture content is observed in pre-monsoon. Moreover, increased LAI is observed during this time at KNP due to the growth of new leaves (Deb Burman et al., 2017). Hence, LE grows with VPD at a faster rate during this season due to the increased combination of evaporation and transpiration both. Finally, after reaching the critical value it decreases due to stomatal closure (Gyenge et al., 2003). On the other hand, withdrawal of monsoonal wind happens in post-monsoon resulting in the gradual decrease of moisture content in the atmosphere. LAI also starts to decrease during post-monsoon (Deb Burman et al., 2017). As a result of this evapotranspiration is hindered and hence, does not increase with VPD. This is manifested in the saturation of LE with VPD. During night time in

all the seasons, convective activities reduce in the absence of solar heating. Additionally, sap flow also reduces in the plants bringing the transpiration down. As a combined effect of both of these LE decreases monotonically with VPD during night time.

5 Conclusions

The seasonal variation of surface energy budget has been studied for the first time in a tropical forest over north-east India using a year-round ground based observation of meteorological variables and EC fluxes during 2016. Surface energy budget closure is seen to vary widely among different seasons with maximum closure of 76% in pre-monsoon and minimum closure of 62% in winter. During Indian summer monsoon a closure of 68% is recorded, while 72% closure is observed in post-monsoon. Annual closure obtained was 70% and 80% using half-hourly and daily values, respectively. Evapotranspiration plays an important role in the closure process. The closure of surface energy budget is seen to be linked with the relative strengths of the sensible and latent heat fluxes. The worst closure is observed at the highest value of Bowen ratio, during winter and the best closure is observed at the smaller value of Bowen ratio in monsoon. Photosynthetic photon flux density and vapour pressure deficit exhibit close controls on evapotranspiration which vary markedly among different seasons. In order to gain a deeper understanding of the controls of evapotranspiration, we plan to partition it into evaporation and transpiration and subsequently study the effects of meteorological, radiation, and soil parameters on both of these separately in our future studies.

Acknowledgements

We express our sincere gratitude to the Director, IITM for all his constant encouragement and support. We thank all the members of the project team for all possible help. CCCR (Centre for Climate Change Research) is part of Indian Institute of Tropical Meteorology, Pune

(IITM) and is fully supported by Earth System Science Organization (ESSO) of Ministry of Earth Sciences (MoES), Government of India.

References

Admiral, S.W., Lafleur, P.M., Roulet, N.T., 2006. Controls on latent heat flux and energy partitioning at a peat bog in eastern Canada. *Agric. For. Meteorol.* **140**, 308–321. https://doi.org/10.1016/j.agrformet.2006.03.017

Anderson, M.C., Norman, J.M., Meyers, T.P., Diak, G.R., 2000. An analytical model for estimating canopy transpiration and carbon assimilation fluxes based on canopy light-use efficiency. *Agric. For. Meteorol.* **101**, 265–289. https://doi.org/10.1016/S0168-1923(99)00170-7

Anthoni, P.M., Unsworth, M.H., Law, B.E., Irvine, J., Baldocchi, D.D., Van Tuyl, S., Moore, D., 2002. Seasonal differences in carbon and water vapor exchange in young and old-growth ponderosa pine ecosystems. *Agric. For. Meteorol.* **111**, 203–222. https://doi.org/10.1016/S0168-1923(02)00021-7

Aubinet, M., Vesala, T., Papale, D., 2012. *Eddy covariance: a practical guide to measurement and data analysis*. Springer, New York, https://doi.org/10.1007/978-94-007-2351-1

Baldocchi, D., 2014. Measuring fluxes of trace gases and energy between ecosystems and the atmosphere – the state and future of the eddy covariance method. *Glob. Chang. Biol.* **20**, 3600–3609. https://doi.org/10.1111/gcb.12649

Baldocchi, D., Falge, E., Gu, L., Olson, R., others, 2001. FLUXNET: A new tool to study the temporal and spatial variability of ecosystem-scale carbon dioxide, water vapor, and energy flux densities. *Bull. Am. Meteorol. Soc.* **82**, 2415. https://doi.org/10.1175/1520-0477(2001)082<2415:FANTTS>2.3.CO;2

Bhat, G.S., Arunchandra, S.C., 2009. On the measurement of the surface energy budget over a land surface during the summer monsoon. *J. Earth Syst. Sci.* **117**, 911–923. https://doi.org/10.1007/s12040-008-0076-0

Bhat, G.S., Narasimha, R., 2007. Indian summer monsoon experiments. *Curr. Sci.* **93**, 153–164.

Bovard, B.D., Curtis, P.S., Vogel, C.S., Su, H.-B., Schmid, H.P., 2005. Environmental controls on sap flow in a northern hardwood forest. *Tree Physiol.* **25**, 31–38. https://doi.org/10.1093/treephys/25.1.31

Bréda, N.J.J., 2003. Ground-based measurements of leaf area index: a review of methods, instruments and current controversies. *J. Exp. Bot.* **54**, 2403–2417. https://doi.org/10.1093/jxb/erg263

Brümmer, C., Falk, U., Papen, H., Szarzynski, J., Wassmann, R., Brüggemann, N., 2008. Diurnal, seasonal, and interannual variation in carbon dioxide and energy exchange in shrub savanna in Burkina Faso (West Africa). *J. Geophys. Res. Biogeosciences* **113**. https://doi.org/10.1029/2007JG000583

Burba, G., 2013. Eddy covariance method for scientific, industrial, agricultural and regulatory applications: A field book on measuring ecosystem gas exchange and areal emission rates. LI-Cor Biosciences.

Caird, M.A., Richards, J.H., Donovan, L.A., 2007. Nighttime stomatal conductance and transpiration in C3 and C4 plants. *Plant Physiol.* **143**, 4–10. https://doi.org/10.1104/pp.106.092940

Chatterjee, A., Roy, A., Chakraborty, S., Karipot, A.K., Sarkar, C., Singh, S., Ghosh, S.K., Mitra, A., Raha, S., 2018. Biosphere Atmosphere Exchange of CO2, H2O Vapour and Energy during Spring over a High Altitude Himalayan Forest at Eastern India. *Aerosol Air Qual. Res.* 1–16. https://doi.org/10.4209/aaqr.2017.12.0605

Cho, J., Oki, T., Yeh, P.J.-F., Kim, W., Kanae, S., Otsuki, K., 2012. On the relationship between the Bowen ratio and the near-surface air temperature. *Theor. Appl. Climatol.* **108**, 135–145. https://doi.org/10.1007/s00704-011-0520-y

Daughtry, C.S.T., Kustas, W.P., Moran, M.S., Pinter, P.J., Jackson, R.D., Brown, P.W., Nichols, W.D., Gay, L.W., 1990. Spectral estimates of net radiation and soil heat flux. *Remote Sens. Environ.* **32**, 111–124. https://doi.org/10.1016/0034-4257(90)90012-B

Dawson, T.E., Burgess, S.S.O., Tu, K.P., Oliveira, R.S., Santiago, L.S., Fisher, J.B., Simonin, K.A., Ambrose, A.R., 2007. Nighttime transpiration in woody plants from contrasting ecosystems. *Tree Physiol.* **27**, 561–575. https://doi.org/10.1093/treephys/27.4.561

de Silans, A.P., Monteny, B.A., Lhomme, J.P., 1997. The correction of soil heat flux measurements to derive an accurate surface energy balance by the Bowen ratio method. *J. Hydrol.* **188**, 453–465. https://doi.org/10.1016/S0022-1694(96)03187-3

Deb Burman, P.K., Sarma, D., Williams, M., Karipot, A., Chakraborty, S., 2017. Estimating gross primary productivity of a tropical forest ecosystem over north-east India using LAI and meteorological variables. *J. Earth Syst. Sci.* **126**, 1–16. https://doi.org/10.1007/s12040-017-0874-3

Dirmeyer, P.A., Gao, X., Zhao, M., Guo, Z., Oki, T., Hanasaki, N., 2006. GSWP-2: Multimodel analysis and implications for our perception of the land surface. *Bull. Am. Meteorol. Soc.* **87**, 1381–1397. https://doi.org/10.1175/BAMS-87-10-1381

Dugas, W.A., Fritschen, L.J., Gay, L.W., Held, A.A., Matthias, A.D., Reicosky, D.C., Steduto, P., Steiner, J.L., 1991. Bowen ratio, eddy correlation, and portable chamber measurements of sensible and latent heat flux over irrigated spring wheat. *Agric. For. Meteorol.* **56**, 1–20. https://doi.org/10.1016/0168-1923(91)90101-U

Eamus, D., Hutley, L.B., O'Grady, A.P., 2001. Daily and seasonal patterns of carbon and water fluxes above a north Australian savanna. *Tree Physiol.* **21**, 977–988. https://doi.org/10.1093/treephys/21.12-13.977

Finkelstein, P.L., Sims, P.F., 2001. Sampling error in eddy correlation flux measurements. *J. Geophys. Res.* https://doi.org/10.1029/2000JD900731

Fisher, J.B., Baldocchi, D.D., Misson, L., Dawson, T.E., Goldstein, A.H., 2007. What the towers don't see at night: nocturnal sap flow in trees and shrubs at two AmeriFlux sites in California. *Tree Physiol.* **27**, 597–610. https://doi.org/10.1093/treephys/27.4.597

Fisher, J.B., Malhi, Y., Bonal, D., Da Rocha, H.R., De Araujo, A.C., Gamo, M., Goulden, M.L., Hirano, T., Huete, A.R., Kondo, H., others, 2009. The land--atmosphere water flux in the tropics. *Glob. Chang. Biol.* **15**, 2694–2714. https://doi.org/10.1111/j.1365-

2486.2008.01813.x

Fisher, R.A., Williams, M., de Lourdes Ruivo, M., de Costa, A.L., Meir, P., 2008. Evaluating climatic and soil water controls on evapotranspiration at two Amazonian rainforest sites. *Agric. For. Meteorol.* **148**, 850–861. https://doi.org/10.1016/j.agrformet.2007.12.001

Foken, T., Aubinet, M., Finnigan, J.J., Leclerc, M.Y., Mauder, M., Paw U, K.T., 2011. Results of a panel discussion about the energy balance closure correction for trace gases. *Bull. Am. Meteorol. Soc.* **92**, ES13--ES18. https://doi.org/10.1175/2011BAMS3130.1

Foken T., Göockede M., Mauder M., Mahrt L., Amiro B., Munger W. (2004) Post-Field Data Quality Control. In: Lee X., Massman W., Law B. (eds) *Handbook of Micrometeorology*. Atmospheric and Oceanographic Sciences Library, vol 29. Springer, Dordrecht. https://doi.org/10.1007/1-4020-2265-4_9

Frolking, S.E. et al, 1998. The relationship between ecosystem productivity and photosynthetically active radiation for northern peatlands. *Global Biogeochem. Cycles* **12**, 115–126.

Gadgil, S., Gadgil, S., 2006. The Indian monsoon, GDP and agriculture. *Econ. Polit. Wkly.* 4887–4895. https://doi.org/10.2307/4418949

Giambelluca, T.W., Martin, R.E., Asner, G.P., Huang, M., Mudd, R.G., Nullet, M.A., DeLay, J.K., Foote, D., 2009. Evapotranspiration and energy balance of native wet montane cloud forest in Hawai ‘i. *Agric. For. Meteorol.* **149**, 230–243. https://doi.org/10.1016/j.agrformet.2008.08.004

Goldstein, A.H., Hultman, N.E., Fracheboud, J.M., Bauer, M.R., Panek, J.A., Xu, M., Qi, Y., Guenther, A.B., Baugh, W., 2000. Effects of climate variability on the carbon dioxide, water, and sensible heat fluxes above a ponderosa pine plantation in the Sierra Nevada (CA). *Agric. For. Meteorol.* **101**, 113–129. https://doi.org/10.1016/S0168-1923(99)00168-9

Goswami, B.N., Ajayamohan, R.S., 2001. Intraseasonal oscillations and interannual variability of the Indian summer monsoon. *J. Clim.* **14**, 1180–1198. https://doi.org/10.1175/1520-0442(2001)014<1180:IOAIVO>2.0.CO;2

Greco, S., Baldocchi, D.D., 1996. Seasonal variations of CO2 and water vapour exchange rates over a temperate deciduous forest. *Glob. Chang. Biol.* **2**, 183–197. https://doi.org/10.1111/j.1365-2486.1996.tb00071.x

Gu, L., Meyers, T., Pallardy, S.G., Hanson, P.J., Yang, B., Heuer, M., Hosman, K.P., Riggs, J.S., Sluss, D., Wullschleger, S.D., 2006. Direct and indirect effects of atmospheric conditions and soil moisture on surface energy partitioning revealed by a prolonged drought at a temperate forest site. *J. Geophys. Res. Atmos.* **111**. https://doi.org/10.1029/2006JD007161

Gu, S., Tang, Y., Cui, X., Kato, T., Du, M., Li, Y., Zhao, X., 2005. Energy exchange between the atmosphere and a meadow ecosystem on the Qinghai--Tibetan Plateau. *Agric. For. Meteorol.* **129**, 175–185. https://doi.org/10.1016/j.agrformet.2004.12.002

Gyenge, J.E., Fernández, M.E., Schlichter, T.M., 2003. Water relations of ponderosa pines in Patagonia Argentina: implications for local water resources and individual growth.

Trees-structure Funct. **17**, 417–423. https://doi.org/10.1007/s00468-003-0254-2

Heusinkveld, B.G., Jacobs, A.F.G., Holtslag, A.A.M., Berkowicz, S.M., 2004. Surface energy balance closure in an arid region: role of soil heat flux. *Agric. For. Meteorol.* **122**, 21–37. https://doi.org/10.1016/j.agrformet.2003.09.005

Hingane, L.S., Rupa Kumar, K., Ramana Murty, B. V., 1985. Long- term trends of surface air temperature in india. *J. Climatol.* **5**, 521–528. https://doi.org/10.1002/joc.3370050505

Hogg, E.H., Hurdle, P.A., 1997. Sap flow in trembling aspen: implications for stomatal responses to vapor pressure deficit. *Tree Physiol.* **17**, 501–509. https://doi.org/10.1093/treephys/17.8-9.501

Idso, S.B., Aase, J.K., Jackson, R.D., 1975. Net Radiation - soil heat flux relations as influenced by soil water content variations. *Boundary-Layer Meteorol.* **9**, 113–122. https://doi.org/10.1007/BF00232257

Jain, S.K., Kumar, V., 2012. Trend analysis of rainfall and temperature data for India. *Curr. Sci.* **102**, 37–49.

Jarvis, P.G., Massheder, J.M., Hale, S.E., Moncrieff, J.B., Rayment, M., Scott, S.L., 1997. Seasonal variation of carbon dioxide, water vapor, and energy exchanges of a boreal black spruce forest. *J. Geophys. Res. Atmos.* **102**, 28953–28966. https://doi.org/10.1029/97JD01176

Jasechko, S., Sharp, Z.D., Gibson, J.J., Birks, S.J., Yi, Y., Fawcett, P.J., 2013. Terrestrial water fluxes dominated by transpiration. *Nature* **496**, 347–350. https://doi.org/10.1038/nature11983

Jha, C.S., Thumaty, K.C., Rodda, S.R., Sonakia, A., Dadhwal, V.K., 2013. Analysis of carbon dioxide, water vapour and energy fluxes over an Indian teak mixed deciduous forest for winter and summer months using eddy covariance technique. *J. earth Syst. Sci.* **122**, 1259–1268. https://doi.org/10.1007/s12040-013-0350-7

Jhajharia, D., Shrivastava, S.K., Sarkar, D., Sarkar, S., 2009. Temporal characteristics of pan evaporation trends under the humid conditions of northeast India. *Agric. For. Meteorol.* **149**, 763–770. https://doi.org/10.1016/j.agrformet.2008.10.024

Jung, M., Reichstein, M., Margolis, H.A., Cescatti, A., Richardson, A.D., Arain, M.A., Arneth, A., Bernhofer, C., Bonal, D., Chen, J., others, 2011. Global patterns of land-atmosphere fluxes of carbon dioxide, latent heat, and sensible heat derived from eddy covariance, satellite, and meteorological observations. *J. Geophys. Res. Biogeosciences* **116**. https://doi.org/10.1029/2010JG001566

Kaimal, J.C., Finnigan, J.J., 1994. Atmospheric boundary layer flows: their structure and measurement. Oxford University Press.

Kool, D., Agam, N., Lazarovitch, N., Heitman, J.L., Sauer, T.J., Ben-Gal, A., 2014. A review of approaches for evapotranspiration partitioning. *Agric. For. Meteorol.* **184**, 56–70. https://doi.org/10.1016/j.agrformet.2013.09.003

Kottek, M., Grieser, J., Beck, C., Rudolf, B., Rubel, F., 2006. World map of the Köppen-Geiger climate classification updated. *Meteorol. Zeitschrift* **15**, 259–263.

https://doi.org/10.1127/0941-2948/2006/0130

Kustas, W.P., Daughtry, C.S.T., 1990. Estimation of the soil heat flux/net radiation ratio from spectral data. *Agric. For. Meteorol.* **49**, 205–223. https://doi.org/10.1016/0168-1923(90)90033-3

Kustas, W.P., Daughtry, C.S.T., Van Oevelen, P.J., 1993. Analytical treatment of the relationships between soil heat flux/net radiation ratio and vegetation indices. *Remote Sens. Environ.* **46**, 319–330. https://doi.org/10.1016/0034-4257(93)90052-Y

Lawrence, D.M., Thornton, P.E., Oleson, K.W., Bonan, G.B., 2007. The partitioning of evapotranspiration into transpiration, soil evaporation, and canopy evaporation in a GCM: impacts on land--atmosphere interaction. *J. Hydrometeorol.* **8**, 862–880. https://doi.org/10.1175/JHM596.1

Leuning, R., Van Gorsel, E., Massman, W.J., Isaac, P.R., 2012. Reflections on the surface energy imbalance problem. *Agric. For. Meteorol.* **156**, 65–74. https://doi.org/10.1016/j.agrformet.2011.12.002

Malek, E., Bingham, G.E., 1993. Comparison of the Bowen ratio-energy balance and the water balance methods for the measurement of evapotranspiration. *J. Hydrol.* **146**, 209–220. https://doi.org/10.1016/0022-1694(93)90276-F

Mauder, M., Cuntz, M., Drüe, C., Graf, A., Rebmann, C., Schmid, H.P., Schmidt, M., Steinbrecher, R., 2013. A strategy for quality and uncertainty assessment of long-term eddy-covariance measurements. *Agric. For. Meteorol.* **169**, 122–135. https://doi.org/10.1016/j.agrformet.2012.09.006

Mauder, M., Foken, T., 2006. Impact of post-field data processing on eddy covariance flux estimates and energy balance closure. *Meteorol. Zeitschrift* **15**, 597–609. https://doi.org/10.1127/0941-2948/2006/0167

Moffat, A.M., Papale, D., Reichstein, M., Hollinger, D.Y., Richardson, A.D., Barr, A.G., Beckstein, C., Braswell, B.H., Churkina, G., Desai, A.R., others, 2007. Comprehensive comparison of gap-filling techniques for eddy covariance net carbon fluxes. *Agric. For. Meteorol.* **147**, 209–232. https://doi.org/10.1016/j.agrformet.2007.08.011

Moncrieff J., Clement R., Finnigan J., Meyers T. (2004) Averaging, Detrending, and Filtering of Eddy Covariance Time Series. In: Lee X., Massman W., Law B. (eds) *Handbook of Micrometeorology*. Atmospheric and Oceanographic Sciences Library, vol 29. Springer, Dordrecht. https://doi.org/10.1007/1-4020-2265-4_2

Moncrieff, J.B., Massheder, J.M., de Bruin, H., Elbers, J., Friborg, T., Heusinkveld, B., Kabat, P., Scott, S., Soegaard, H., Verhoef, a., 1997. A system to measure surface fluxes of momentum, sensible heat, water vapour and carbon dioxide. *J. Hydrol.* **188–189**, 589–611. https://doi.org/10.1016/S0022-1694(96)03194-0

Monteith, J.L., 1965. Evaporation and the environment. In: *The State and Movement of Water in Living Organisms* (ed.) Fogg G E, Symp. Soc. Exp. Biol., 19. Cambridge University Press, London.

Mukhopadhyay, P., Jaswal, A., Deshpande, M., 2017. Variability and Trends of Atmospheric Moisture over the Indian Region, in: Rajeevan, M., Nayak, S. (Eds.), Observed Climate

Variability and Change over the Indian Region. Springer, pp. 129–144. https://doi.org/10.1007/978-981-10-2531-0_8

Nakai, T., der Molen, M.K., Gash, J.H.C., Kodama, Y., 2006. Correction of sonic anemometer angle of attack errors. *Agric. For. Meteorol.* **136**, 19–30. https://doi.org/10.1016/j.agrformet.2006.01.006

Norman, J.M., Kustas, W.P., Prueger, J.H., Diak, G.R., 2000. Surface flux estimation using radiometric temperature: A dual temperature-difference method to minimize measurement errors. *Water Resour. Res.* **36**, 2263–2274. https://doi.org/Doi 10.1029/2000wr900033

Novick, K.A., Oren, R., Stoy, P.C., Siqueira, M.B.S., Katul, G.G., 2009. Nocturnal evapotranspiration in eddy-covariance records from three co-located ecosystems in the Southeastern US: implications for annual fluxes. *Agric. For. Meteorol.* **149**, 1491–1504. https://doi.org/10.1016/j.agrformet.2009.04.005

Papale, D., Reichstein, M., Aubinet, M., Canfora, E., Bernhofer, C., Kutsch, W., Longdoz, B., Rambal, S., Valentini, R., Vesala, T., others, 2006. Towards a standardized processing of Net Ecosystem Exchange measured with eddy covariance technique: algorithms and uncertainty estimation. *Biogeosciences* **3**, 571–583. https://doi.org/10.5194/bg-3-571-2006

Parthasarathy, B., Munot, A.A., Kothawale, D.R., 1994. All-India monthly and seasonal rainfall series: 1871-1993. *Theor. Appl. Climatol.* **49**, 217–224. https://doi.org/10.1007/BF00867461

Parthasarathy, B., Rupa Kumar, K., Sontakke, N.A., 1990. Surface and upper air temperatures over India in relation to monsoon rainfall. *Theor. Appl. Climatol.* **42**, 93–110. https://doi.org/10.1007/BF00868216

Pejam, M.R., Arain, M.A., McCaughey, J.H., 2006. Energy and water vapour exchanges over a mixedwood boreal forest in Ontario, Canada. *Hydrol. Process.* **20**, 3709–3724. https://doi.org/10.1002/hyp.6384

Pieruschka, R., Huber, G., Berry, J.A., 2010. Control of transpiration by radiation. *Proc. Natl. Acad. Sci.* **107**, 13372–13377. https://doi.org/10.1073/pnas.0913177107

Purdy, A.J., Fisher, J.B., Goulden, M.L., Famiglietti, J.S., 2016. Ground heat flux: An analytical review of 6 models evaluated at 88 sites and globally. *J. Geophys. Res. Biogeosciences* **121**, 3045–3059. https://doi.org/10.1002/2016JG003591

Ramana, M.V., Krishnan, P., Kunhikrishnan, P.K., 2004. Surface boundary-layer characteristics over a tropical inland station: Seasonal features. *Boundary-Layer Meteorol.* **111**, 153–175. https://doi.org/10.1023/B:BOUN.0000010999.25921.1a

Ramier, D., Boulain, N., Cappelaere, B., Timouk, F., Rabanit, M., Lloyd, C.R., Boubkraoui, S., Métayer, F., Descroix, L., Wawrzyniak, V., 2009. Towards an understanding of coupled physical and biological processes in the cultivated Sahel--1. Energy and water. *J. Hydrol.* **375**, 204–216. https://doi.org/10.1016/j.jhydrol.2008.12.002

Randerson, J.T., Chapin, F.S., Harden, J.W., Neff, J.C., Harmon, M.E., 2002. Net ecosystem production: a comprehensive measure of net carbon accumulation by ecosystems. *Ecol.*

Appl. **12**, 937–947. https://doi.org/10.1890/1051-0761(2002)012[0937:NEPACM]2.0.CO;2

Reddy, N.N., Rao, K.G., 2018. Contrasting variations in the surface layer structure between the convective and non-convective periods in the summer monsoon season for Bangalore location during PRWONAM. *J. Atmos. Solar-Terrestrial Phys.* **167**, 156–168. https://doi.org/10.1016/j.jastp.2017.11.017

Reichstein, M., Falge, E., Baldocchi, D., Papale, D., Aubinet, M., Berbigier, P., Bernhofer, C., Buchmann, N., Gilmanov, T., Granier, A., others, 2005. On the separation of net ecosystem exchange into assimilation and ecosystem respiration: review and improved algorithm. *Glob. Chang. Biol.* **11**, 1424–1439. https://doi.org/10.1111/j.1365-2486.2005.001002.x

Reverter, B.R., Sánchez-Cañete, E.P., Resco, V., Serrano-Ortiz, P., Oyonarte, C., Kowalski, A.S., 2010. Analyzing the major drivers of NEE in a Mediterranean alpine shrubland. *Biogeosciences* **7**, 2601–2611. https://doi.org/10.5194/bg-7-2601-2010

Rodda, S.R., Thumaty, K.C., Jha, C.S., Dadhwal, V.K., 2016. Seasonal Variations of Carbon Dioxide, Water Vapor and Energy Fluxes in Tropical Indian Mangroves. *Forests* **7**, 35. https://doi.org/10.3390/f7020035

Rothfuss, Y., Biron, P., Braud, I., Canale, L., Durand, J., Gaudet, J., Richard, P., Vauclin, M., Bariac, T., 2010. Partitioning of Evapotranspiration Into Soil Evaporation and Plant Partitioning evapotranspiration fluxes into soil evaporation and plant transpiration using water stable isotopes under controlled conditions. *Hydrol. Process.* **24**, 3177–3194. https://doi.org/10.1002/hyp.7743

Sachs, L., 1997. Angewandte Statistik: Anwendung statistischer Methoden. Springer.

Sakai, R.K., Fitzjarrald, D.R., Moore, K.E., 2001. Importance of low-frequency contributions to eddy fluxes observed over rough surfaces. *J. Appl. Meteorol.* **40**, 2178–2192.

Sauer, T.J., Ochsner, T.E., Horton, R., 2007. Soil Heat Flux Plates. *Agron. J.* **99**, 304–310. https://doi.org/10.2134/agronj2005.0038s

Scott, R.L., Edwards, E.A., Shuttleworth, W.J., Huxman, T.E., Watts, C., Goodrich, D.C., 2004. Interannual and seasonal variation in fluxes of water and carbon dioxide from a riparian woodland ecosystem. *Agric. For. Meteorol.* **122**, 65–84. https://doi.org/10.1016/j.agrformet.2003.09.001

Sellers, P.J., 1987. Canopy reflectance, photosynthesis, and transpiration, II. The role of biophysics in the linearity of their interdependence. *Remote Sens. Environ.* **21**, 143–183. https://doi.org/10.1016/0034-4257(87)90051-4

Shi, T.-T., Guan, D.-X., Wu, J.-B., Wang, A.-Z., Jin, C.-J., Han, S.-J., 2008. Comparison of methods for estimating evapotranspiration rate of dry forest canopy: Eddy covariance, Bowen ratio energy balance, and Penman-Monteith equation. *J. Geophys. Res. Atmos.* **113**. https://doi.org/10.1029/2008JD010174

Shuttleworth, W.J., 2007. Putting the "vap" into evaporation. *Hydrol. Earth Syst. Sci.* **11**, 210–244. https://doi.org/10.5194/hess-11-210-2007

Si, J.-H., Feng, Q., Zhang, X.-Y., Chang, Z.-Q., Su, Y.-H., Xi, H., 2007. Sap Flow of

\textit{Populus euphratica} in a desert riparian forest in an extreme arid region during the growing season. *J. Integr. Plant Biol.* **49**. https://doi.org/10.1111/j.1744-7909.2007.00388.x

Sikka, D.R., Narasimha, R., 1995. Genesis of the monsoon trough boundary layer experiment (MONTBLEX). *Proc. Indian Acad. Sci. Planet. Sci.* (Earth Planet Sci.) **104**, 157–187. https://doi.org/10.1007/BF02839270

Singh, O.P., Ali Khan, T.M., Rahman, M.S., 2000. Changes in the frequency of tropical cyclones over the North Indian Ocean. *Meteorol. Atmos. Phys.* **75**, 11–20. https://doi.org/10.1007/s007030070011

Stull, R.B., 2012. *An introduction to boundary layer meteorology*, vol 13. Springer, Dordrecht. https://doi.org/10.1007/978-94-009-3027-8

Tanner, C., 1960. Energy balance approach to evapotranspiration from crops. *Soil Sci. Soc. Am. J.* **24**, 1–9. https://doi.org/10.2136/sssaj1960.03615995002400010012x

Tsai, J.-L., Tsuang, B.-J., Lu, P.-S., Chang, K.-H., Yao, M.-H., Shen, Y., 2010. Measurements of aerodynamic roughness, Bowen ratio, and atmospheric surface layer height by eddy covariance and tethersonde systems simultaneously over a heterogeneous rice paddy. *J. Hydrometeorol.* **11**, 452–466. https://doi.org/10.1175/2009JHM1131.1

Twine, T.E., Kustas, W.P., Norman, J.M., Cook, D.R., Houser, Pr., Meyers, T.P., Prueger, J.H., Starks, P.J., Wesely, M.L., 2000. Correcting eddy-covariance flux underestimates over a grassland. *Agric. For. Meteorol.* **103**, 279–300. https://doi.org/10.1016/S0168-1923(00)00123-4

Vernekar, K.G., Sadani, L.K., Sivaramakrishnan, S., Parasnis, S.S., Mohan, B., Saxena, S., Dharmaraj, T., Patil, M.N., Pillai, J.S., Murthy, B.S., Debaje, S.B., Bagavathsingh, A., 2003. An Overview of the Land Surface Processes Experiment (LASPEX) over a Semi-Arid Region of India. *Boundary-Layer Meteorol. 106 Issue 3 pp* **2003**, 561–572. https://doi.org/10.1023/A:1021283503661

Wang, B., 2006. The asian monsoon. Springer, Heidelberg. https://doi.org/10.1007/3-540-37722-0

Wang, B., Ho, L., 2002. Rainy season of the Asian-Pacific summer monsson. *J. Clim.* **15**, 386–398. https://doi.org/10.1175/1520-0442(2002)015<0386:RSOTAP>2.0.CO;2

Wang, J., Yu, Q., Li, J., Li, L.-H., Li, X.-G., Yu, G.-R., Sun, X.-M., 2006. Simulation of diurnal variations of CO 2, water and heat fluxes over winter wheat with a model coupled photosynthesis and transpiration. *Agric. For. Meteorol.* **137**, 194–219. https://doi.org/10.1016/j.agrformet.2006.02.007

Wang, K., Dickinson, R.E., 2012. A review of global terrestrial evapotranspiration: Observation, modeling, climatology, and climatic variability. *Rev. Geophys.* **50**. https://doi.org/10.1029/2011RG000373

Watham, T., Kushwaha, S.P.., Patel, N.R., Dadhwal, V.K., 2014. Monitoring of carbon dioxide and water vapour exchange over a young mixed forest plantation using eddy covariance technique. *Curr. Sci.* **107**, 858–866.

Webb, E.K., Pearman, G.I., Leuning, R., 1980. Correction of flux measurements for density

effects due to heat and water vapour transfer. *Q. J. R. Meteorol. Soc.* **106**, 85–100. https://doi.org/10.1002/qj.49710644707

Wilson, K., Goldstein, A., Falge, E., Aubinet, M., Baldocchi, D., Berbigier, P., Bernhofer, C., Ceulemans, R., Dolman, H., Field, C., others, 2002. Energy balance closure at FLUXNET sites. *Agric. For. Meteorol.* **113**, 223–243. https://doi.org/10.1016/S0168-1923(02)00109-0

Wilson, K.B., Baldocchi, D.D., 2000. Seasonal and interannual variability of energy fluxes over a broadleaved temperate deciduous forest in North America. *Agric. For. Meteorol.* **100**, 1–18. https://doi.org/10.1016/S0168-1923(99)00088-X

Wutzler, T., Lucas-Moffat, A., Migliavacca, M., Knauer, J., Sickel, K., Šigut, L., Menzer, O., Reichstein, M., 2018. Basic and extensible post-processing of eddy covariance flux data with REddyProc. *Biogeosciences Discuss.* **15**, 1–39. https://doi.org/10.5194/bg-2018-56

Xavier, P.K., Marzin, C., Goswami, B.N., 2007. An objective definition of the Indian summer monsoon season and a new perspective on the ENSO-monsoon relationship. *Q. J. R. Meteorol. Soc.* **133**, 749–764. https://doi.org/10.1002/qj.45

Yang, K., Wang, J., 2008. A temperature prediction-correction method for estimating surface soil heat flux from soil temperature and moisture data. *Sci. China Ser. D Earth Sci.* **51**, 721–729. https://doi.org/10.1007/s11430-008-0036-1

Yaseef, N.R., Yakir, D., Rotenberg, E., Schiller, G., Cohen, S., 2010. Ecohydrology of a semi-arid forest: partitioning among water balance components and its implications for predicted precipitation changes. *Ecohydrology* **3**, 143–154. https://doi.org/10.1002/eco.65

Table 1: Instruments and Variables used. Depths within the soil are marked as negative.

Instrument	Model and manufacturer	Altitude of measurement (m)	Variable (unit)	Temporal resolution (s)	Accuracy
multi-component weather sensor	WXT520, Vaisala Oyj., Vantaa, Finland	4, 7, 20, 37	T_a (K), P (hPa), precip (mm)	60	±0.3 K for T_a, ±0.5 hPa for P and ≤ 5% for precip
3-D sonic anemometer-thermometer	WindMaster Pro, Gill Instruments, Lymington, UK	37	u (m s^{-1}), v (m s^{-1}), w (m s^{-1})	0.1	< 1.5% RMS (Root Mean Square)
CO_2 and H_2O Infrared Gas Analyzers	IRGA Model: LI-7200 enclosed path CO_2/H_2O analyzer, Li-COR Biosciences, Lincoln, USA	37	c (µmol m^{-3}), q (g kg^{-1})	0.1	within 1% and 2% of readings for CO_2 and H_2O measurements, respectively
4-component net radiometer	NR01, Hukseflux, Manorville, NY, USA	19	R_{SW}(in) (W m^{-2}), R_{LW}(in) (W m^{-2}), R_{SW}(out) (W m^{-2}), R_{LW}(out) (W m^{-2}), R_n (W m^{-2})	60	< 15 W m^{-2}
quantum sensor	SQ-110, Apogee Instruments, Inc., Logan, Utah, USA	19	PPFD (µmol m^{-3})	60	±5%
soil heat flux plate	HFP01SC-20, Campbell Scientific, Logan, Utah, USA	-0.05	G (W m-2)	60	±3%

Table 2: Biometeorological variables required for quality control and gap filling of the flux data. Depths within the soil are marked as negative.

Variable (unit)	Instrument	Model and manufacturer	Altitude/depth of measurement (m)	Temporal resolution (m)	Accuracy
T_a (K)	multi-component weather sensor	WXT520, Vaisala Oyj., Vantaa, Finland	4, 7, 20, 37	1, 30	±0.3 K
P (hPa)	multi-component weather sensor	WXT520, Vaisala Oyj., Vantaa, Finland	4, 7, 20, 37	1, 30	±0.5 hPa
RH (%)	multi-component weather sensor	WXT520, Vaisala Oyj., Vantaa, Finland	4, 7, 20, 37	1, 30	±3\%
T_s (K)	water content, electrical conductivity and temperature sensor	5TE, Decagon Devices Inc., Pullman, Washington, USA	surface, -0.05, -0.15, -0.25, -0.40	1, 30	±1 K
SWC ($m^3\ m^{-3}$)	water content, electrical conductivity and temperature sensor	5TE, Decagon Devices Inc., Pullman, Washington, USA	surface, -0.05, -0.15, -0.25, -0.40	1, 30	±15\%

Table 3: SEB closure, residual energy and β during different seasons.

Season (months)	SEB closure (%)	Residual energy flux (W m^{-2})	β (at 12.0 h)
pre-monsoon (MAM)	76	8.53	0.33
monsoon (JJAS)	68	5.11	0.27
post-monsoon (ON)	72	15.36	0.37
winter (DJF)	62	15.55	0.93

Figure Captions

1. Map of India showing the location (tower symbol) of the micrometeorological flux tower at Kaziranga national park (KNP) in north-east India.
2. Annual variations of (a) daily averaged air temperature (T_a), (b) daily averaged air pressure (P), and (c) daily total precipitation (precip) at Kaziranga national park (KNP) for 2016. Different seasons are indicated at the top of the figure.
3. Scatter plot between half-hourly values of net radiation (R_n) and latent heat flux (LE) observed at KNP during 2016.
4. Surface Energy Budget (SEB) closure at KNP for 2016 using half-hourly averaged values of net radiation (R_n), sensible heat flux (H), latent heat flux (LE), and soil heat flux (G). G has been parameterised from R_n.
5. Scatter plots and linear fits between net radiation (R_n) and soil heat flux (G) during (a) day time and (b) night time for KNP in 2016. Daytime is defined using (R_{SW}(in)) > 20 W m^{-2}. Governing equation for each of the fits is given in the respective figure legends.
6. Surface Energy Budget (SEB) closure at KNP for 2016 using half-hourly averaged values of net radiation (R_n), sensible heat flux (H), latent heat flux (LE), and soil heat flux (G). G has been parameterised from R_n.
7. Surface Energy Budget (SEB) closure at KNP for 2016 using daily averaged values of net radiation (R_n), sensible heat flux (H), latent heat flux (LE), and soil heat flux (G). G has been parameterised from R_n.
8. Mean diurnal variations of net radiation (R_n), incoming shortwave radiation (R_{SW}(in)), sensible heat flux (H), and latent heat flux (LE) at KNP during 2016 for (a) pre-monsoon, (b) monsoon, (c) post-monsoon, and (d) winter. The x-axes and y-axes in all the sub-plots show the time in hour (local time) and the different energy fluxes in

$W\ m^{-2}$.

9. Surface Energy Budget (SEB) closure at KNP for (a) pre-monsoon (March-April-May or MAM), (b) monsoon (June-July-August-September or JJAS), (c) post-monsoon (October-November or ON), and (d) winter (December-January-February or DJF) during 2016 using half-hourly averaged values of net radiation (R_n), sensible heat flux (H), latent heat flux (LE), and soil heat flux (G). G has been parameterised from R_n. Red continuous lines represent the ideal closure with unit slope. Blue continuous lines represent the linear fits between (R_n - G) and (H + LE) as obtained from the data using least-square method. Governing equation and the adjusted R-squared value for each of the fits are given in the respective figure legends.
10. Scatter plots and linear fits between Photosynthetic Photon Flux Density (PPFD) and latent heat flux (LE) during (a) pre-monsoon (March-April-May or MAM), (b) monsoon (June-July-August-September or JJAS), (c) post-monsoon (October-November or ON), and (d) winter (December-January-February or DJF) at KNP during 2016. Blue lines represent the linear fit between PPFD and LE as obtained by least-square method for different seasons. Regression equations and determination coefficients are provided on each panel.
11. Scatter plots between vapour pressure deficit (VPD) and latent heat flux (LE) during (a) pre-monsoon (March-April-May or MAM), (b) monsoon (June-July-August-September or JJAS), (c) post-monsoon (October-November or ON), and (d) winter (December-January-February or DJF) in 2016 at KNP. Temporal trend proceeds clockwise in all the plots. Continuous lines represent the fits to the scatter plots during the time when LE increases with VPD.

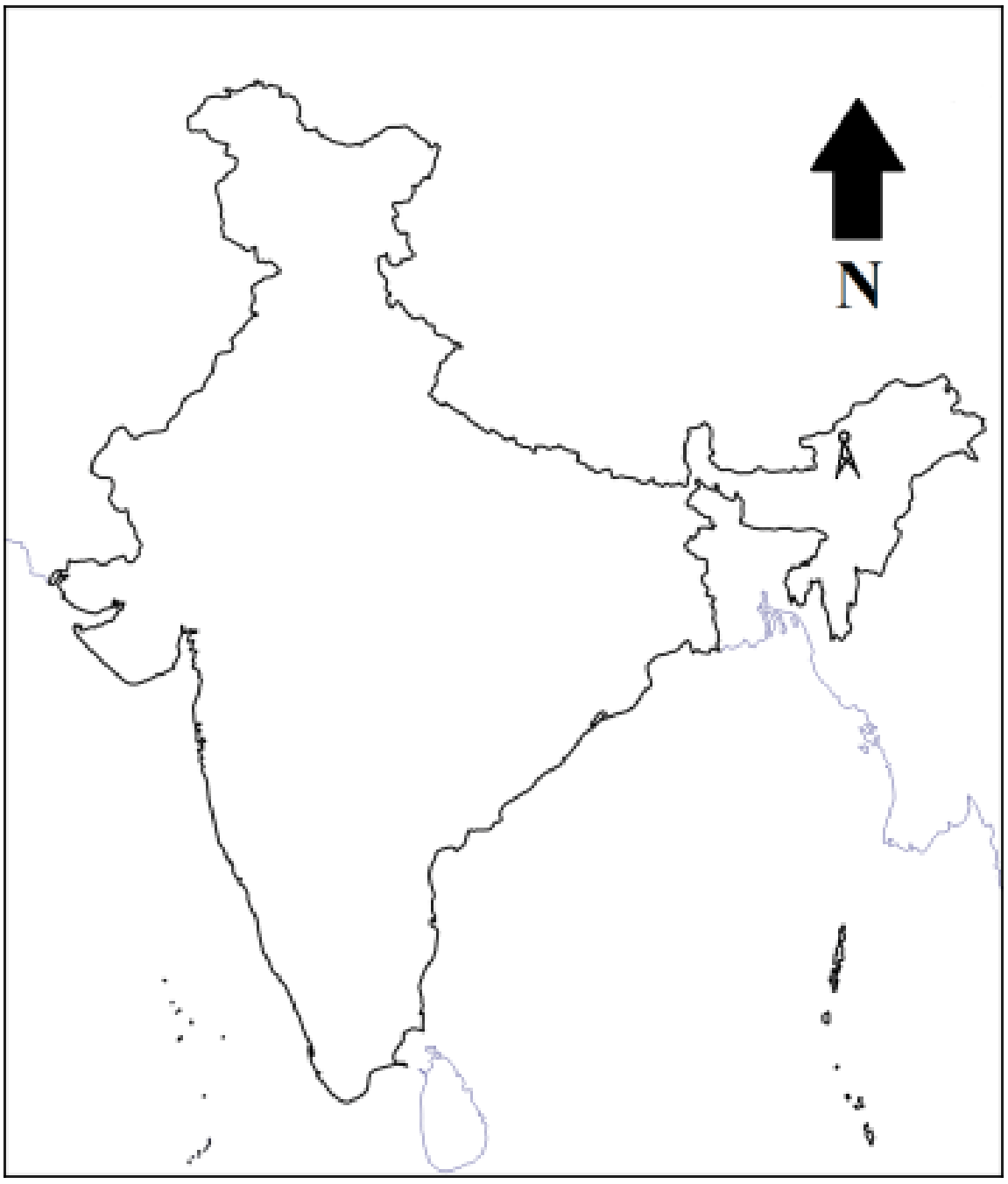

1. Map of India showing the location (tower symbol) of the micrometeorological flux tower at Kaziranga national park (KNP) in north-east India.

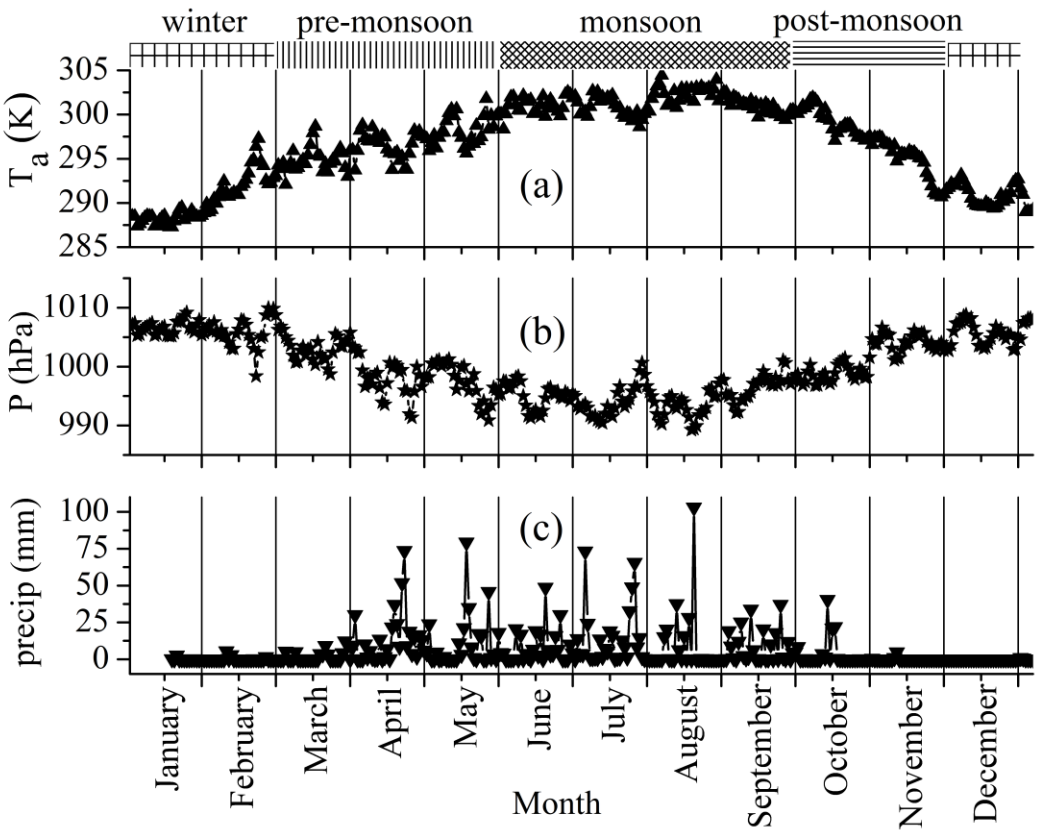

2. Annual variations of (a) daily averaged air temperature (T_a), (b) daily averaged air pressure (P), and (c) daily total precipitation (precip) at Kaziranga national park (KNP) for 2016. Different seasons are indicated at the top of the figure.

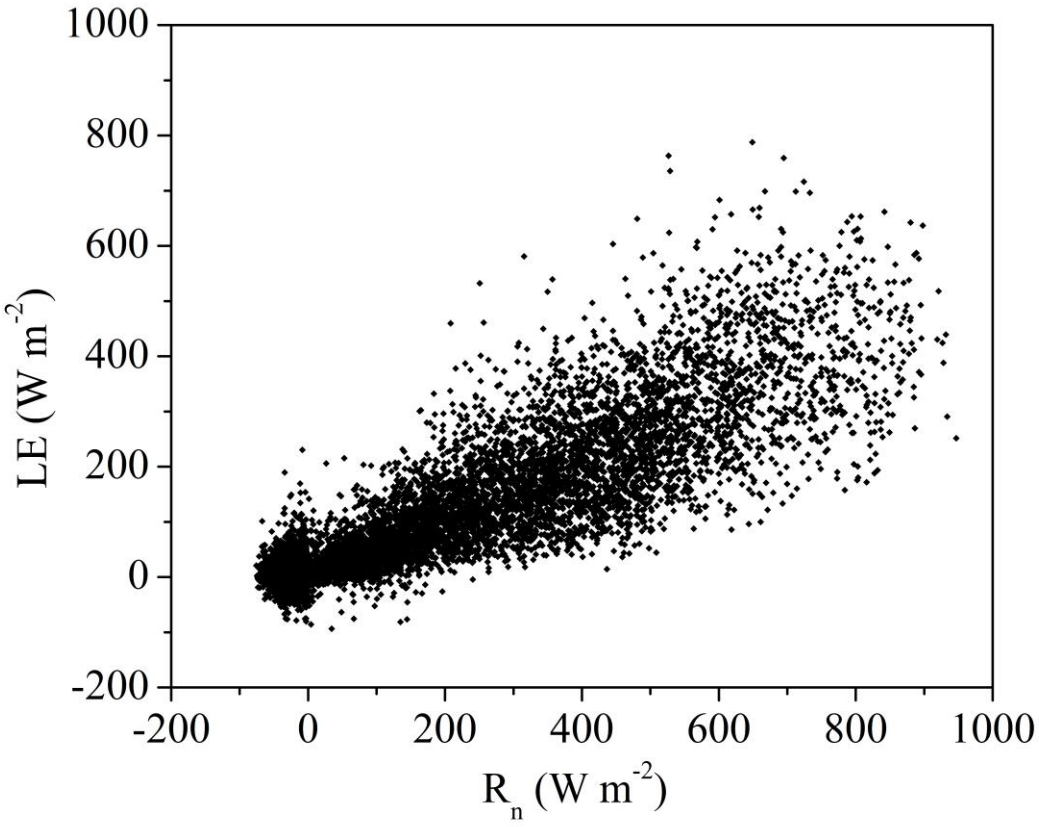

3. Scatter plot between half-hourly values of net radiation (R_n) and latent heat flux (LE) observed at KNP during 2016.

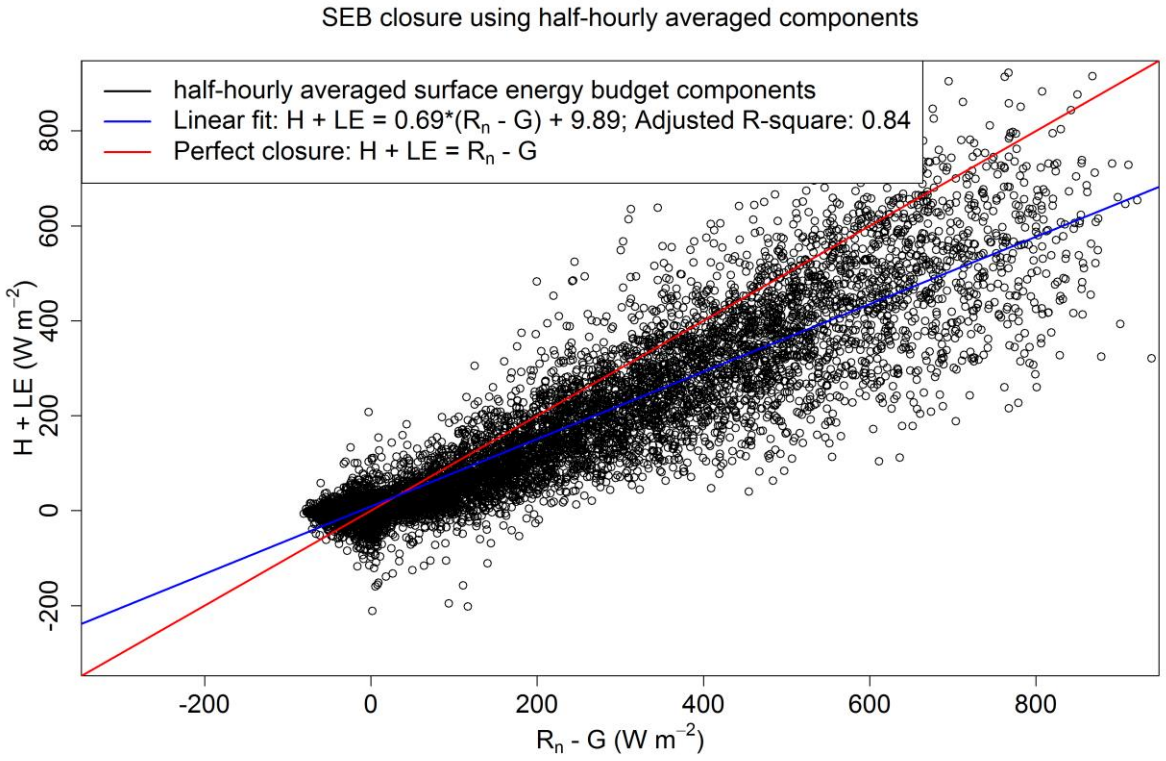

4. Surface Energy Budget (SEB) closure at KNP for 2016. Data are thirty minute averages of net radiation (R_n), sensible heat flux (H), latent heat flux (LE), and soil heat flux (G).

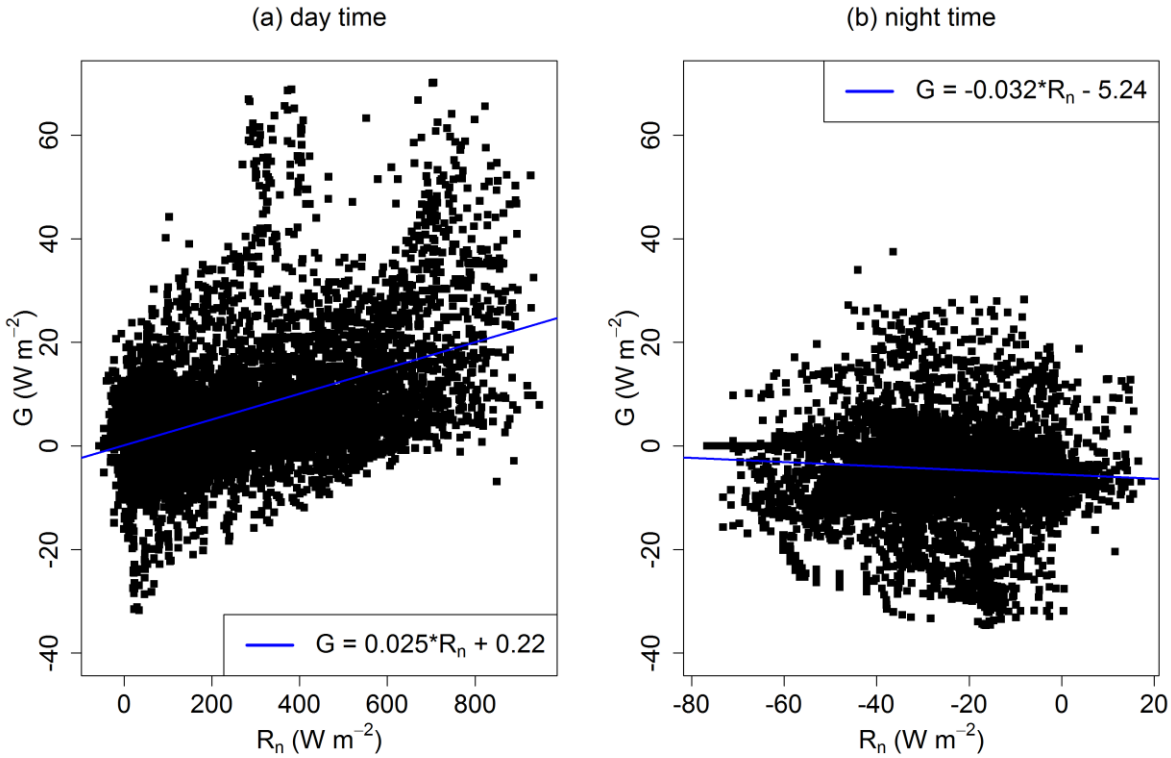

5. Scatter plots and linear fits between net radiation (R_n) and soil heat flux (G) during (a) day time and (b) night time for KNP in 2016. Daytime is defined using (R_{SW}(in)) > 20 W m^{-2}. Governing equation for each of the fits is given in the respective figure legends.

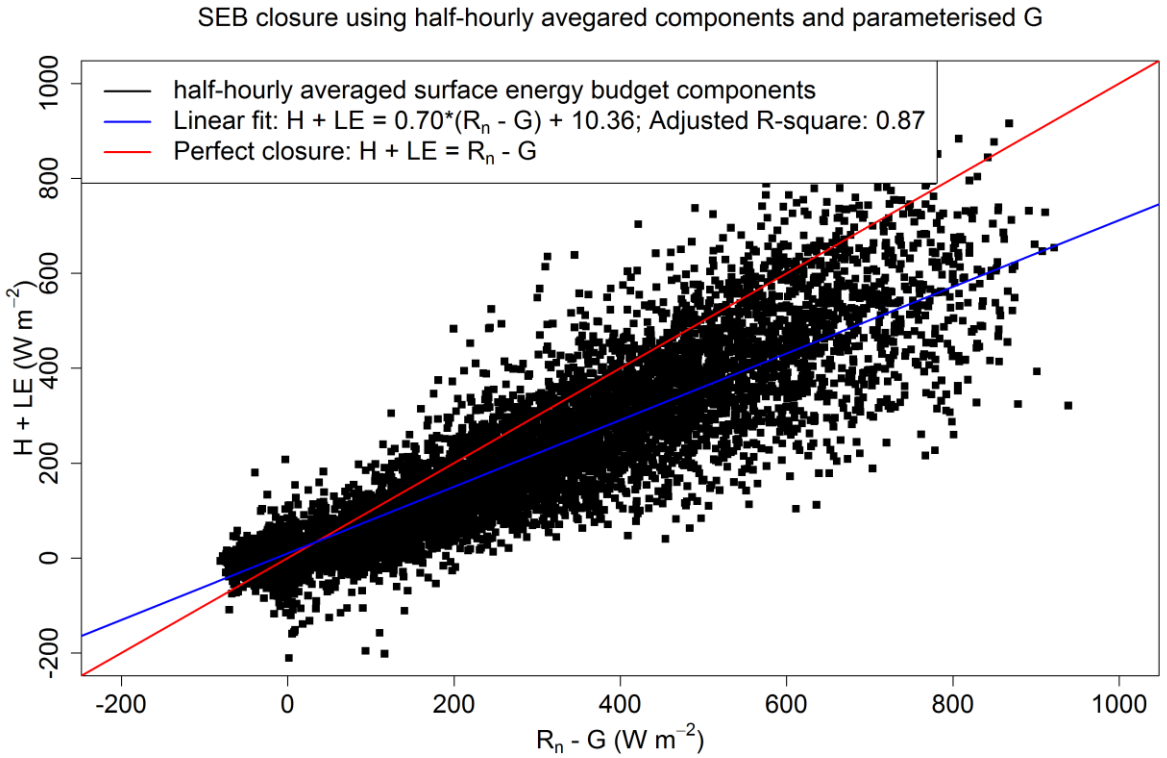

6. Surface Energy Budget (SEB) closure at KNP for 2016 using half-hourly averaged values of net radiation (R_n), sensible heat flux (H), latent heat flux (LE), and soil heat flux (G). G has been parameterised from R_n.

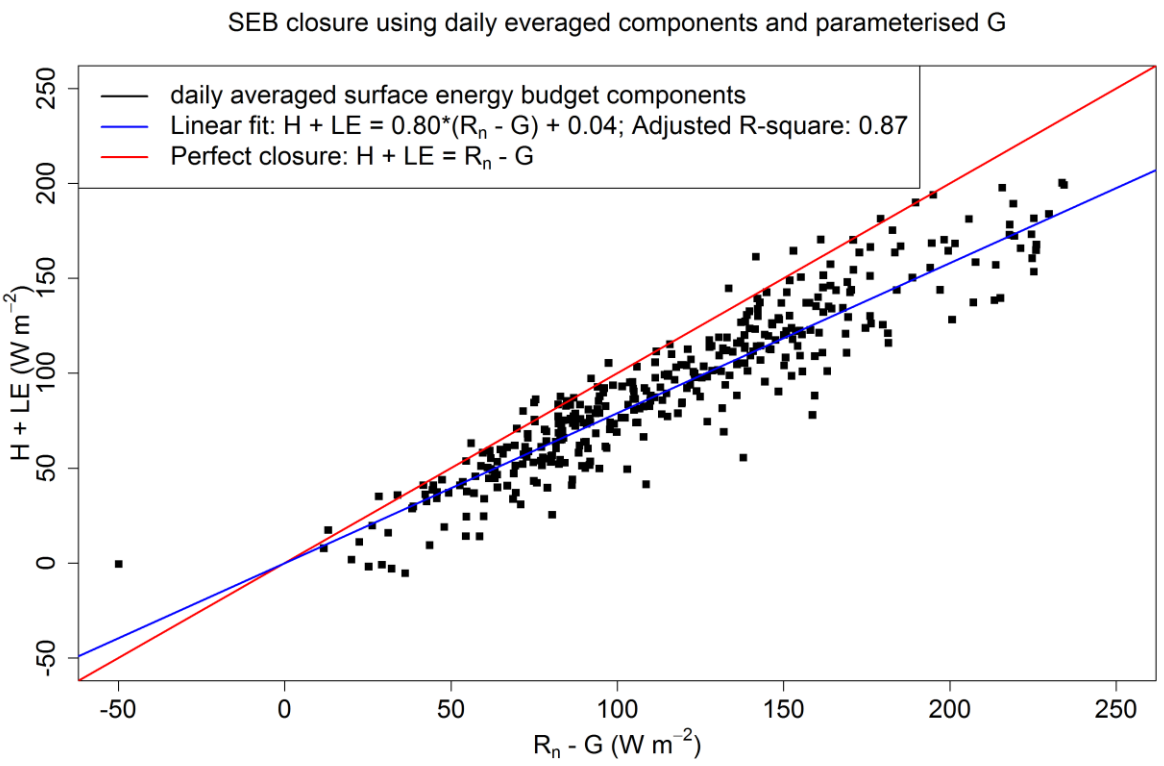

7. Surface Energy Budget (SEB) closure at KNP for 2016 using daily averaged values of net radiation (R_n), sensible heat flux (H), latent heat flux (LE), and soil heat flux (G). G has been parameterised from R_n.

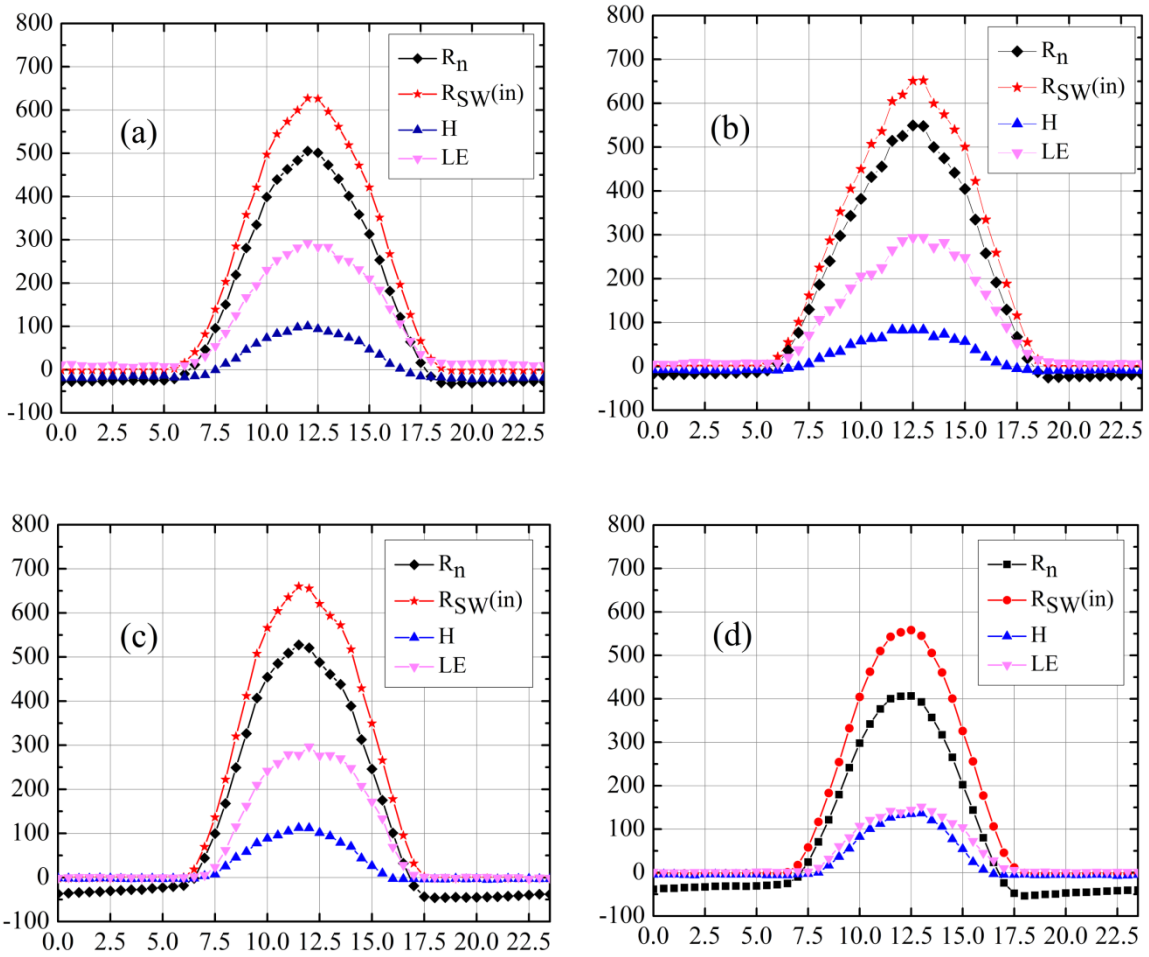

8. Mean diurnal variations of net radiation (R_n), incoming shortwave radiation ($R_{SW}(in)$), sensible heat flux (H), and latent heat flux (LE) at KNP during 2016 for (a) pre-monsoon, (b) monsoon, (c) post-monsoon, and (d) winter. The x-axes and y-axes in all the sub-plots show the time in hour (local time) and the different energy fluxes in W m^{-2}.

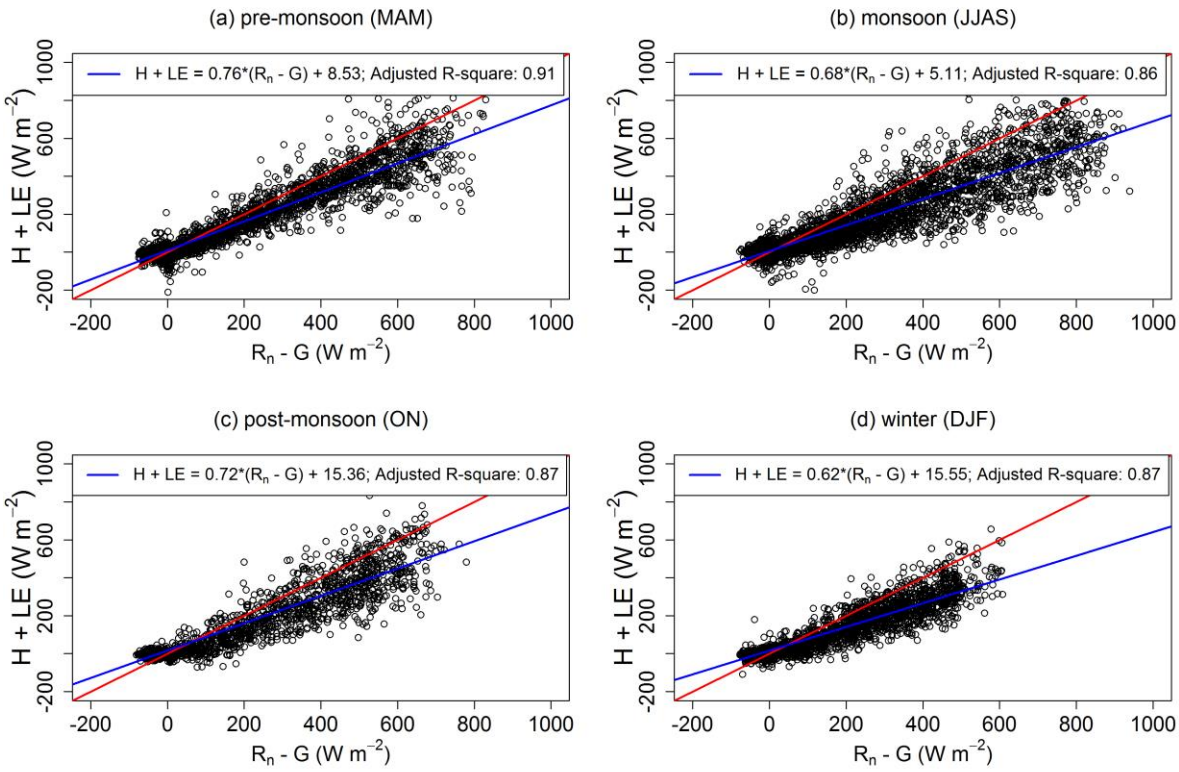

9. Surface Energy Budget (SEB) closure at KNP for (a) pre-monsoon (March-April-May or MAM), (b) monsoon (June-July-August-September or JJAS), (c) post-monsoon (October-November or ON), and (d) winter (December-January-February or DJF) during 2016 using half-hourly averaged values of net radiation (R_n), sensible heat flux (H), latent heat flux (LE), and soil heat flux (G). G has been parameterised from R_n. Red continuous lines represent the ideal closure with unit slope. Blue continuous lines represent the linear fits between (R_n - G) and (H + LE) as obtained from the data using least-square method. Governing equation and the adjusted R-squared value for each of the fits are given in the respective figure legends.

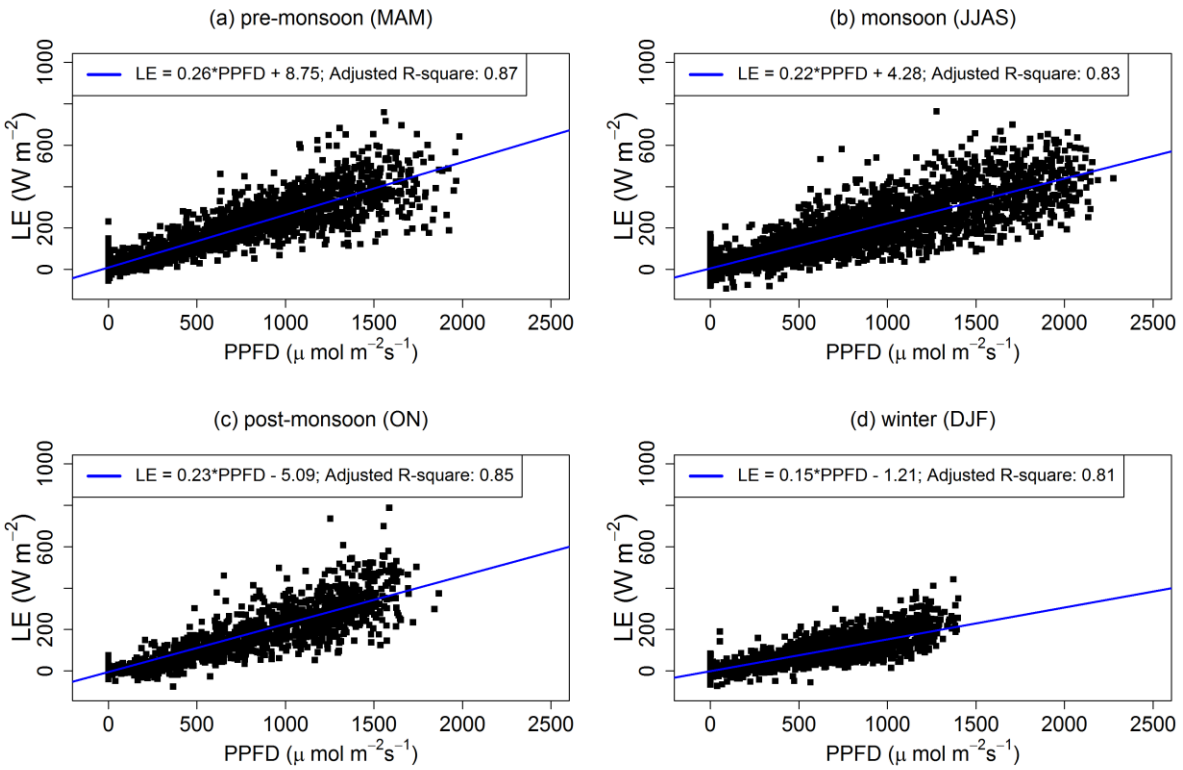

10. Scatter plots and linear fits between Photosynthetic Photon Flux Density (PPFD) and latent heat flux (LE) during (a) pre-monsoon (March-April-May or MAM), (b) monsoon (June-July-August-September or JJAS), (c) post-monsoon (October-November or ON), and (d) winter (December-January-February or DJF) at KNP during 2016. Blue lines represent the linear fit between PPFD and LE as obtained by least-square method for different seasons. Regression equations and determination coefficients are provided on each panel.

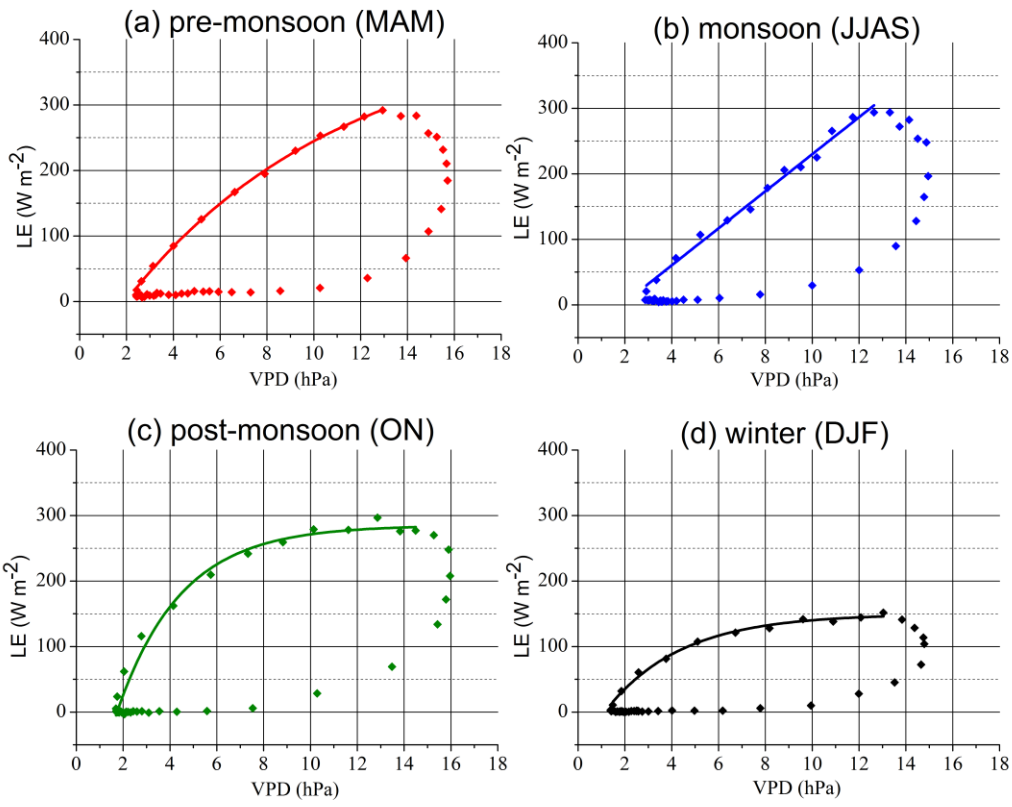

11. Scatter plots between vapour pressure deficit (VPD) and latent heat flux (LE) during (a) pre-monsoon (March-April-May or MAM), (b) monsoon (June-July-August-September or JJAS), (c) post-monsoon (October-November or ON), and (d) winter (December-January-February or DJF) in 2016 at KNP. Temporal trend proceeds clockwise in all the plots. Continuous lines represent the fits to the scatter plots during the time when LE increases with VPD.